



Record 2016/10 | eCat 89869

Evaluation of the TanDEM-X Intermediate DEM for Terrain Illumination Correction in Landsat Data

F. Li, D.L.B. Jupp, M. Thankappan, L.W. Wang, A. Lewis and A. Held

Evaluation of the TanDEM-X Intermediate DEM for Terrain Illumination Correction in Landsat Data

GEOSCIENCE AUSTRALIA
RECORD 2016/10

F. Li¹, D.L.B. Jupp², M. Thankappan¹, L.W. Wang¹, A. Lewis¹ and A. Held²



1. Geoscience Australia
2. CSIRO, Land and Water

D Department of Industry, Innovation and Science

Minister for Resources, Energy and Northern Australia: The Hon Josh Frydenberg MP

Assistant Minister for Science: The Hon Karen Andrews MP

Secretary: Ms Glenys Beauchamp PSM

Geoscience Australia

Chief Executive Officer: Dr Chris Pigram

This paper is published with the permission of the CEO, Geoscience Australia



© Commonwealth of Australia (Geoscience Australia) 2016

With the exception of the Commonwealth Coat of Arms and where otherwise noted, this product is provided under a Creative Commons Attribution 4.0 International Licence.

(<http://creativecommons.org/licenses/by/4.0/legalcode>)

Geoscience Australia has tried to make the information in this product as accurate as possible. However, it does not guarantee that the information is totally accurate or complete. Therefore, you should not solely rely on this information when making a commercial decision.

Geoscience Australia is committed to providing web accessible content wherever possible. If you are having difficulties with accessing this document please email clientservices@gov.au.

ISSN 2201-702X (PDF)

ISBN 978-1-925297-05-8 (PDF)

eCat 89869

Bibliographic reference: Li, F., Jupp, D.L.B., Thankappan, M., Wang, L.W., Lewis, A. & Held, A. 2016. *Evaluation of the TanDEM-X Intermediate DEM for Terrain Illumination Correction in Landsat Data*. Record 2016/10. Geoscience Australia, Canberra. <http://dx.doi.org/10.11636/Record.2016.010>

Contents

| | |
|---|----|
| Executive Summary..... | iv |
| 1 Introduction..... | 1 |
| 2 Method and models used | 4 |
| 2.1 Terrain illumination correction model..... | 4 |
| 2.2 Scale analysis of the data correlation | 6 |
| 3 Study area and data description..... | 8 |
| 3.1 Study area..... | 8 |
| 3.2 Data..... | 9 |
| 3.2.1 DEM/DSM data | 9 |
| 3.2.2 Landsat data..... | 10 |
| 3.2.3 Ancillary data | 10 |
| 4 Results and discussion..... | 11 |
| 4.1 Initial assessment of the IDEM data | 11 |
| 4.2 Results from terrain illumination studies | 13 |
| 4.3 Results from Filter Bank analysis | 29 |
| 5 Conclusions & Evaluation..... | 36 |
| Acknowledgements | 37 |
| References | 38 |

Executive Summary

Terrain illumination correction is an important step in the normalisation of remotely sensed data for the inversion of land surface parameters, and for applications that aim to detect land surface change through time series analysis. An appropriate resolution of the Digital Elevation Model (DEM) data with sufficient quality is critical for effective correction of remotely sensed data over mountainous areas. Conversely, using terrain illumination correction and scale-based analysis, such as filter bank analysis, the quality of DEM data can be evaluated relative to the scale of the target data. In this study, TanDEM-X Intermediate DEM (IDEM) data at 12 m and 30 m resolutions, and the 1-arc second Shuttle Radar Topography Mission (SRTM) data (\sim 30 m resolution) were used to evaluate their absolute and relative effectiveness in terrain illumination correction for Landsat satellite optical data.

The island of Tasmania in Australia has significant local terrain detail as well as high regional relief. This, together with its high latitude and wide variation in terrain illumination throughout the year, makes it an ideal study site to test correction methods and assess different resolution candidate DEM data. A set of images from both Landsat 7 and 8 multispectral bands (MS) and panchromatic (Pan) band were collected. These images were put through standard atmospheric and BRDF processing as well as terrain illumination correction using different sources of DEM. Comparisons were made by undertaking terrain correction with the various input DEMs and using visual and difference image methods to evaluate them. Quantitative Filter Bank analysis is also used to evaluate performance as a function of spatial scale. In total, five DEMs were used for the study, which include three at Landsat MS scale (derived from 12m and 30m IDEM and 1 sec SRTM data) and two at Landsat Pan scale (derived from 12m IDEM and 1 sec SRTM data).

Results from the terrain illumination correction and filter bank analysis show that (provided the analysis is confined to areas without some specific data issues), although all data sets can carry out the task well, the IDEM 12 m resolution based datasets can resolve finer details of terrain shading than the SRTM based DEM. This indicates that IDEM can deliver better results in areas with detail-rich terrain monitored with Landsat data. However, since the data available for this study is a sample from an intermediate product, spikes and other noise artefacts not expected in operational data were prevalent. Noise artefacts occurred especially over areas covered by water. Operational use of the IDEM will require the removal of such noise artefacts, but from the present study we can say if that were fully achieved, the 12m resolution data could form the basis for better terrain correction of Landsat data. The filter bank analysis also found that both Landsat panchromatic data and IDEM 12 m data seem to be over-sampled; studies using even finer DEM data would be required to examine this further.

It should be possible to correct for noise issues, as similar processing was carried out with SRTM data at an early stage to good effect. More detailed evaluation of the relative merits of the TanDEM-X based DEM compared with the SRTM based DEM data for terrain illumination correction may be possible when the WorldDEM™ product based on TanDEM-X data becomes routinely available with the water areas noise issues resolved.

1 Introduction

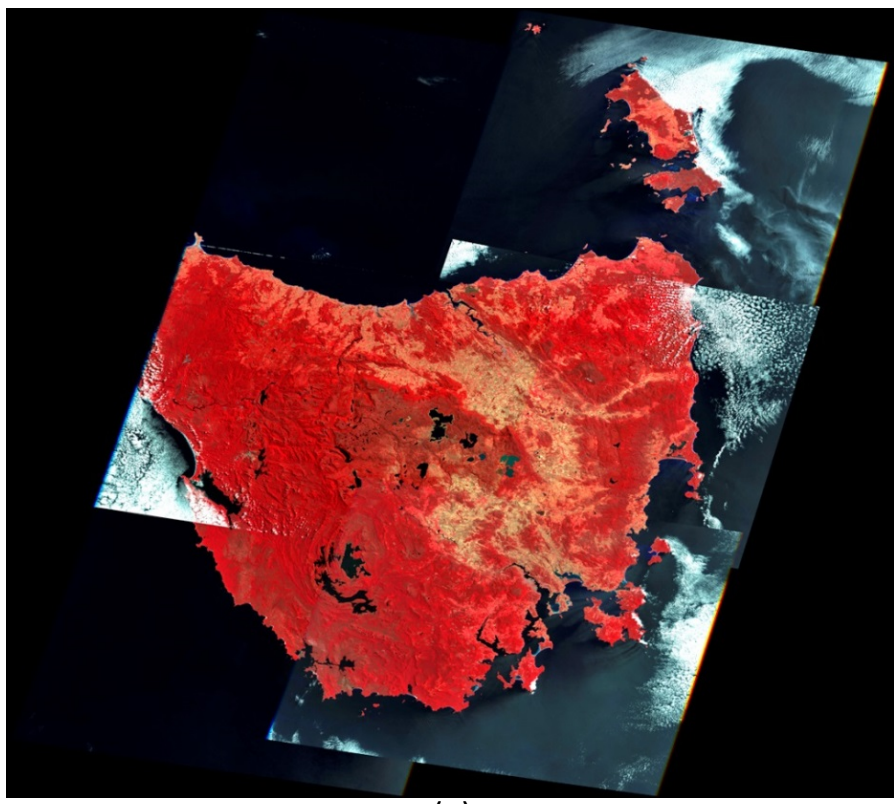
Topographic (terrain illumination) correction is an important step to normalise optical remote sensing data for the inversion of land surface parameters and applications that aim to detect land surface change through time series analysis (Li, et al. 2012). When optical satellite images are sensed in mountainous areas, due to the terrain effect, slopes facing towards the sun receive more solar irradiance and appear brighter than those facing away from the sun. The effect is stronger with anisotropic surfaces where the radiance of sloping surfaces, as viewed by a satellite, is also modified by the surface bidirectional reflectance distribution function (BRDF). This results from surface land cover structure interacting with the sun and satellite geometry (sun and satellite view and its relative azimuth angle) and the terrain geometry (e.g. slope and aspect angles).

To accurately normalise for the terrain effects, an appropriate resolution of DEM data with sufficient quality is critical for effective correction in mountainous areas (Li, et al, 2013). From the DEM data $z(x, y)$, this correction uses the horizontal gradient field:

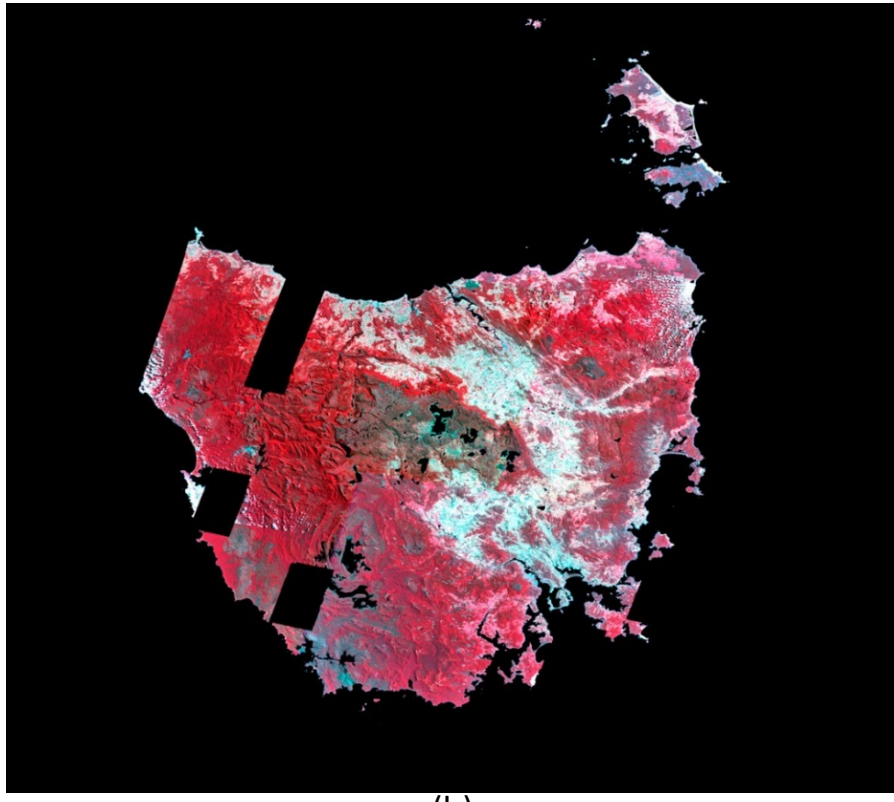
$$\nabla z(x, y) = \left[\frac{\partial z}{\partial x}, \frac{\partial z}{\partial y} \right]$$

The gradient field defines the illumination, slope and aspect that modify the irradiance and causes the terrain effect. Consequently, using terrain illumination modelling and correction, we can evaluate the quality of DEM data. For example, by comparing the corrected with the uncorrected satellite images using different DEMs, the comparative quality of different DEM data sets, such as their response to artefacts and their scale and resolution can be determined. Through scale-based analysis, such as filter bank analysis, we can also assess the matched scale effects in both the remotely sensed and candidate DEM data and assess the quality and sufficiency of one DEM in relation to another. It should be emphasised that this study is based on the gradient field of the DEM and absolute and relative height accuracy are not studied except in some initial qualitative visual comparisons with SRTM data.

In this study, terrain illumination correction and filter bank analysis were used to evaluate the quality of the TanDEM-X Intermediate DEM (IDEM) on the island of Tasmania using eleven Landsat-7 images and one Landsat-8 image. Both 30 m and 12 m resolution TanDEM-X IDEM datasets were evaluated using the similar resolution of the Landsat multispectral bands and panchromatic band respectively. TanDEM-X IDEM is an intermediate DEM and the precursor to the global digital elevation model “WorldDEM™” which specifies an absolute height error of 10m and a relative height error of 2m for 90% of the global land surface (Huber, et al., 2012). The WorldDEM™ product is based on data from the two SAR satellites, TerraSAR-X and TanDEM-X launched in 2007 and 2009 respectively. Being a precursor to the WorldDEM™ product, only the first global coverage was used for generating the IDEM (Huber, et al., 2012). Correction for noise and removal of artefacts over areas covered by water have not yet been done for the IDEM data. For convenience TanDEM-X IDEM is referred to as IDEM in the rest of the report.



(a)



(b)

Figure 1.1 Mosaic images of Landsat over Tasmania, Australia

Figure 1.1 (a) shows a mosaic of nine Landsat scenes used in this study. Only one is Landsat 8. The images have been atmospherically and BRDF corrected but contain significant differences in terrain shading due to the range in times of image acquisition. It is necessary to use images from a range of dates as Tasmania is frequently quite cloudy. The data in Figure 1.1 (b) are the same as (a) but a water mask has been applied to indicate areas not included in terrain correction or comparisons. In addition, areas of missing IDEM data are masked and are visible as angled strips of masked data oriented in a North-South direction. Water masking was essential as the IDEM data had unacceptable noise levels over water covered areas. Results are presented later using the same mosaic pattern.

2 Method and models used

2.1 Terrain illumination correction model

For anisotropic surfaces on mountainous or hilly areas, the radiative transfer model can be expressed as described in Li et al. (2012, 2013):

$$L_{TOA} = L_0 + \frac{T_v}{\pi} \left(E^{dir} [f_v \rho_s(i_t, e_t, \delta\varphi_t) + (1-f_v) \bar{\rho}'(i_t)] + E^{dif} [f_v \bar{\rho}(e_t) + (1-f_v) \bar{\rho}] + E \frac{\bar{\rho}^2}{1 - S\bar{\rho}} \right) \quad (1)$$

$\delta\varphi_t$ is the relative azimuth angle between incident and exiting directions in the slope geometry and $\rho_s(i_t, e_t, \delta\varphi_t)$ is surface reflectance. $\bar{\rho}$, $\bar{\rho}'$ and $\bar{\rho}^2$ are the surface hemispherical-directional, directional-hemispherical and hemispherical-hemispherical reflectance (or bi-hemispherical) factors, respectively, and f_v is the fraction of direct radiation and $f_v = t_v / T_v$. Other symbols are listed in Table 2.1.

Among the terms in Eq. (1), T_v , f_v , L_0 can be obtained through atmospheric correction. The irradiance terms E , E^{dir} and E^{dif} are important for analysis here, particularly the direct irradiance E^{dir} . From the definitions, $E = E^{dir} + E^{dif}$ and the term E^{dir} can be expressed as (Iqbal, 1983; Shepherd and Dymond, 2003; Li, et al., 2012):

$$E^{dir} = E_h^{dir} \Theta \frac{\max(\cos i_t, 0)}{\cos \theta_s} \quad (2)$$

where Θ is a binary coefficient, set to zero in cast shadow (shadow due to obstruction by other parts of the terrain) and set to one otherwise and E_h^{dir} is the direct irradiance on a flat surface and can be estimated through atmospheric correction. Other symbols are listed in Table 2.1. The other expressions for irradiance involve sky occlusion and adjacent scattered irradiance terms (see Li et al., 2012 for details).

The Equations (1)-(2) show that the accuracy of retrieval of surface reflectance from the sloping terrain depends on the accuracy with which the terms such as i_t , e_t , Θ , sky and occlusion factors are computed. These terms in turn depend on the quality of DEM data (Li et al., 2012, 2013).

The incident angle i_t can be found from:

$$\cos i_t = \cos \theta_s \cos \theta_t + \sin \theta_s \sin \theta_t \cos(\phi_s - \phi_t) \quad (3)$$

The exiting angle e_t can be calculated in a similar way.

Table 2.1 Symbols and notations used in this report

| Symbols | Notations |
|--------------------|--|
| θ_s | solar zenith angle |
| ϕ_s | solar azimuth angle |
| θ_t | slope angle |
| ϕ_t | aspect angle of the slope |
| i_t | incident zenith angles between the sun direction and surface normal |
| e_t | existing zenith angles between the view direction and surface normal. |
| t_v | direct transmittance in the view direction |
| S | the atmospheric albedo |
| T_v | total transmittance in the view direction |
| L_{TOA} | sensor radiance at top of atmosphere |
| L_0 | path radiance |
| ρ_s | the surface reflectance (the BRF or bi-directional reflectance factor which is π times the BRDF) |
| E_h^{dir} | the direct component of irradiance on a horizontal surface |
| E | total irradiance on an inclined surface |
| E^{dir} | direct component of irradiance on an inclined surface |
| E^{dif} | diffuse component of irradiance on an inclined surface |

However, to relate this angle directly with the DEM data it is convenient to write it in a different way. Most of the terms needed for the model are obtained from numerical derivatives of the DEM that provide estimates for the components of the gradient field $[p, q]$ where (assuming the DEM estimates the height function $z = z(x, y)$):

$$[p, q] = \nabla z(x, y) = \left[\frac{\partial z}{\partial x}, \frac{\partial z}{\partial y} \right] \quad (4)$$

These numerical estimates can be used to obtain slope and aspect angles but for better understanding of the following analysis, the following terms derived from θ_s and ϕ_s can be defined (Horn and Bachman, 1978):

$$p_s = \sin \theta_s \cot \phi_s \quad (5)$$

$$q_s = \cos \theta_s \cot \phi_s \quad (6)$$

The unit vector for the normal to the terrain (\tilde{n}_t) and the unit vector in the sun direction (\tilde{n}_s) can be expressed as:

$$\tilde{n}_t = \frac{[-p, -q, 1]}{(p^2 + q^2 + 1)^{1/2}} \quad (7)$$

$$\tilde{n}_s = \frac{[-p_s, -q_s, 1]}{(p_s^2 + q_s^2 + 1)^{1/2}} \quad (8)$$

The reason for introducing these expressions is to use them to express $\cos i_t$ in a way that shows its direct relationship with p and q. The result is that:

$$\cos i_t = \tilde{n}_s^T \tilde{n}_t = \frac{1 + p_s p + q_s q}{(1 + p_s^2 + q_s^2)^{1/2} (1 + p^2 + q^2)^{1/2}} \quad (9)$$

This simple and near linear function of the gradient field $[p, q]$ will be used below to assess the DEM quality, scale effects as the image data behave as a similar function of the gradient field of the real earth surface after filtering through the imaging sensor.

2.2 Scale analysis of the data correlation

The roughness of terrain can be expressed by measures such as mean slope or curvature. High curvature areas appear as specific spatial features such as branching streamlines and diverging ridge structures. In image processing, the detail areas are referred to as high frequency components due to their expression as such using Fourier processing (Castleman, 1996). Broad terrain structures such as long catchment slopes and mountain ranges are referred to as low frequency components or trends. It is well-known that, as DEM resolution decreases, mean slopes and curvatures decrease and that terrain details disappear (Wang and Yin, 1998; Yin and Wang, 1999; Wolock and McCabe, 2000). So a DEM will be too coarse if the Landsat image is responding to terrain details not in the DEM and it would be well matched if the significant details are both present and aligned in both.

It is possible to conveniently separate the low and high spatial frequencies using digital image processing (Castleman, 1996). In this study, a set of high pass filters have been used to separate the frequencies into high (detail) and low (trend) components. The application of the high pass filter (H) to the image data (f) can be written:

$$H_h * f = (I - F_h) * f \quad (10)$$

In this expression, F_h is a low pass filter (e.g. smoothing filter) with width h (measured in some cases by the filter Full-Width at Half Maximum or FWHM) and “*” here represents the application of the filter to the data. I is the identity filter defined such that $I * f = f$. The filters are 2-dimensional (to match the image data) and square. The filter used here is slightly different from some other smoothing filters as F_h is the median over a shifting window with side kf (i.e. a square filter of size kf by kf). This has the

advantage of identifying but being less sensitive to outliers when H_h is applied to an image. The width in this case is simply the 1D size of the square window (kf) as the median is unweighted over the filter extent. For small kf most of the lower frequencies will be removed leaving only the finest scale of variation (in this case areas of high local DEM curvature) and for large kf only the broadest trends will be removed leaving the fine and mid-scale spatial frequencies in the resulting image.

Applying the set of filters (H_{kf}) with decreasing kf will provide a set of images whereas kf decreases the image is made up of increasingly finer details. The filter set is applied to the images as follows. If L represents the Landsat image (reflectance obtained without taking shading into account in this study) and C represents a matching image of $\cos i_t$ computed using the DEM, the basic approximate model relationship for shading in band j can be expressed as:

$$L_j \approx a_j + b_j C \quad (11)$$

We can therefore write that:

$$\begin{aligned} H_{kf} * L_j &\approx b_j (H_{kf} * C) \\ \text{var}(H_{kf} * L_j) &\approx b_j^2 \text{ var}(H_{kf} * C) \end{aligned} \quad (12)$$

In this case, “var” refers to the variance of the image component remaining after application of the filter. This will usually decrease as kf reduces since the low frequency (i.e. regional trend) components of images in areas of significant terrain often dominate the total image variance.

In practice, the variances of $H_{kf} * L_j$ and $H_{kf} * C$ will both reduce as kf reduces and the ratio of the variances in each case to that of the total unfiltered image variance should be similar if the two are well related. In addition, if the correlation between the filtered images remains high as kf reduces, the implication is that the fine details (especially the areas with high local curvature) are present and correctly matched in both the (Landsat) image and the DEM data. This filter based analysis will also be applied in this study for scale analysis.

To evaluate this effect, bands with low diffuse radiation and high signal/noise ratio, particularly the near and shortwave infra-red such as Landsat 7 band 4 and Landsat 8 band 5 are used. In these bands, the surface reflectance and the function $\cos i_t$ should be highly correlated in mountainous areas.

3 Study area and data description

3.1 Study area

The island of Tasmania in Australia is the target area for this analysis. Tasmania has a rough terrain with a fine scale of terrain detail as well as high relief. It has a range of landforms, including past glaciations in the high areas, high suspended lakes, areas of high relief and deeply cut river valleys, making it different from most of mainland Australia. Since it is in the mid southern latitudes, the terrain illumination variation is also very strong over the course of a year. Therefore, it is a good area to test the methodology and data sets outlined above. Figure 3.1 shows the area located on an Australian boundary map.

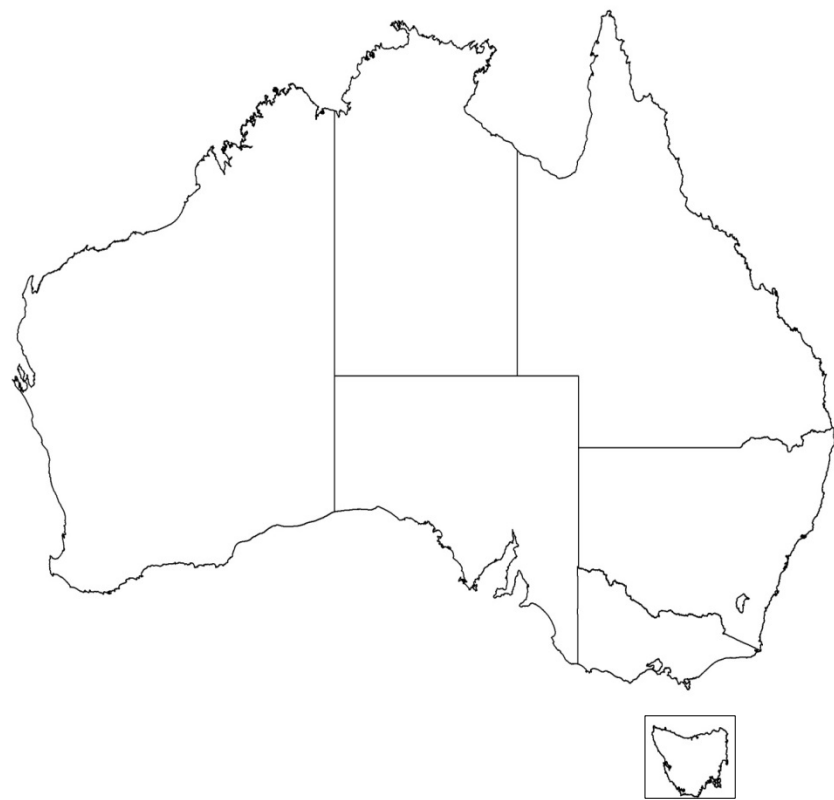


Figure 3.1 Test area over Tasmania (black box) located on an Australian map

3.2 Data

3.2.1 DEM/DSM data

IDEM data were provided by the German Aerospace Center (DLR). The data provided to GA were at nominal 12m, 30m and 90m resolution. Previous work by Li et al. (2012, 2013) showed that the coarser scale 90m SRTM was not adequate for correcting Landsat data for terrain brightness variations associated with irradiance differences on the Australian hill-slopes assessed. For that reason, the 90m data were not considered here and instead, the analysis involved only the 30m and 12m IDEM data sets. The pre-processing used for the IDEM data and its initial quality assessment will be discussed in Section 4.1. For convenience, the IDEM 12 m and 30 m data sets are henceforth referred to as IDEM12 and IDEM30, respectively. Strictly, the resolutions of these data sets are at 0.4 arc second and 1 arc second respectively. All data were processed as Geographic projections in resolution units of degrees. As indicated in Figure 1.1, the study area did not have complete coverage by IDEM data and comparisons were therefore confined to areas where all materials were available and of good quality.

For DEM comparison, a product derived by Geoscience Australia based on 1-arc second SRTM Digital Surface Model (DSM) was used to conduct the terrain illumination and filter bank analysis. The definition of the term “DSM” as used by Geoscience Australia is that the product estimates an effective surface height above sea level which can include areas of trees of sufficient density and other rough surface features. These surface features create an effective “roughness height” for the surface. Since both IDEM and SRTM DSMs respond to the tree cover and other surface feature heights at a similar scale, they are basically comparable although some spatially varying rough height bias between them can be found as the data sets arise from sensors using different Synthetic Aperture Radar (SAR) bands (SRTM is C-band and IDEM is X-Band) and have somewhat different footprints. Satellite images based on other sensors (including optical, thermal and Lidar) also represent radiance referenced to an effective roughness height surface (e.g. tops of canopies or buildings) rather than the soil surface and are therefore generally better related to DSMs than to DEMs. Unfortunately, as the surface roughness layer can change over time there will always be local differences in measured heights between these various sensors. Fortunately, low frequency land cover dependent biases between the three sensor types used in this study are not as serious an issue as other applications based on absolute height because it is the gradient field that is most significant in this study as will be described below. The differences based on sensor frequency are probably less significant than differences arising due to the different imaging dates of the three sensor sets. This is obviously an issue for absolute height comparisons. A full description of the SRTM based product can be found in Gallant et al. (2011). In this report, the 1-arc second SRTM based DSM data set from Geoscience Australia will be denoted as SRTM30.

In previous work involving terrain effect corrections, the SRTM30 data needed to be processed further before being used for terrain correction (Li et al., 2012, 2013). Various artefacts in the data, which can have a significant effect on slope and aspect, needed be removed or reduced. For example, there are cases in the SRTM30 data where the difference between a local median value and the corresponding central pixel exceed 20-30 metres, creating slope outliers. The data were also smoothed using a Gaussian 3 by 3 filter to remove effects due to SRTM originally having a 1 metre vertical precision, and then resampled to Landsat resolution (25m in Australian product) by bilinear interpolation. These and a range of other issues that arise in the use of SRTM30 data in this context have been discussed in greater detail in Li et al. (2013). Similar processing was applied to both the SRTM and the IDEM data in this study as described in Section 4.

3.2.2 Landsat data

Landsat 7 and 8 data are used since both satellites have panchromatic bands which have similar resolution to IDEM12 data, making it ideal to evaluate the quality of IDEM12 data. The Landsat products used here were provided with resolutions of 0.9 arc seconds for the multispectral bands and 0.45 arc seconds for the panchromatic band which are slightly finer than the IDEM30 and slightly coarser resolution than the IDEM12 respectively. Due to the mid southern latitude of Tasmania, winter images were excluded from the analysis because of the high solar zenith angles (low elevation angles) in winter images that create extensive areas of deep shadow in the images making them less useful for the purposes of this study. Tasmania is an area with generally high cloud cover and it is difficult to find completely clear images in a single path/row. However, almost every path/row had two images. Therefore, in total eleven Landsat 7 images and one Landsat 8 image were used for this study (Table 3.1). The data were ortho-corrected by Geoscience Australia to equirectangular projection (latitude and longitude grid, often called a “Geographic” Projection).

Table 3.1 12 Landsat images used in this study

| Image number | Satellite | path | row | Date (Day/month/year) | Solar zenith angle (°) |
|--------------|-----------|------|-----|-----------------------|------------------------|
| 1 | Landsat 7 | 90 | 88 | 30/11/1999 | 33.5 |
| 2 | Landsat 7 | 90 | 88 | 20/02/2001 | 45.9 |
| 3 | Landsat 7 | 90 | 89 | 30/11/1999 | 34.3 |
| 4 | Landsat 7 | 90 | 89 | 09/04/2001 | 60.1 |
| 5 | Landsat 8 | 90 | 89 | 31/01/2014 | 40.2 |
| 6 | Landsat 7 | 90 | 90 | 03/01/2001 | 37.6 |
| 7 | Landsat 7 | 90 | 90 | 03/11/2001 | 39.9 |
| 8 | Landsat 7 | 91 | 88 | 05/03/2003 | 49.4 |
| 9 | Landsat 7 | 91 | 89 | 01/02/2003 | 42.6 |
| 10 | Landsat 7 | 91 | 89 | 05/03/2003 | 50.4 |
| 11 | Landsat 7 | 91 | 90 | 08/01/2000 | 37.8 |
| 12 | Landsat 7 | 91 | 90 | 07/11/2000 | 38.6 |

3.2.3 Ancillary data

In addition to a DEM, the ancillary input data needed to run the terrain illumination correction included atmospheric water vapour, aerosol optical depth, and BRDF parameters. Atmospheric water vapour (the total precipitable water content) data were from the NOAA NCEP (National Centers for Environmental Prediction) reanalysis product (Kalnay et al., 1996). The aerosol data were obtained from CSIRO and derived from AATSR (Qin and Mitchell, 2012). These data sets have been used to correct atmospheric effects in archived Landsat imagery by Geoscience Australia. BRDF parameters were obtained from the MODIS BRDF model product (Schaaf et al., 2002). Following Li et al. (2010, 2012), the BRDF shape is defined for large regions (regional scale). For this study, the average value of BRDF shape over the Landsat scene extent was used.

4 Results and discussion

4.1 Initial assessment of the IDEM data

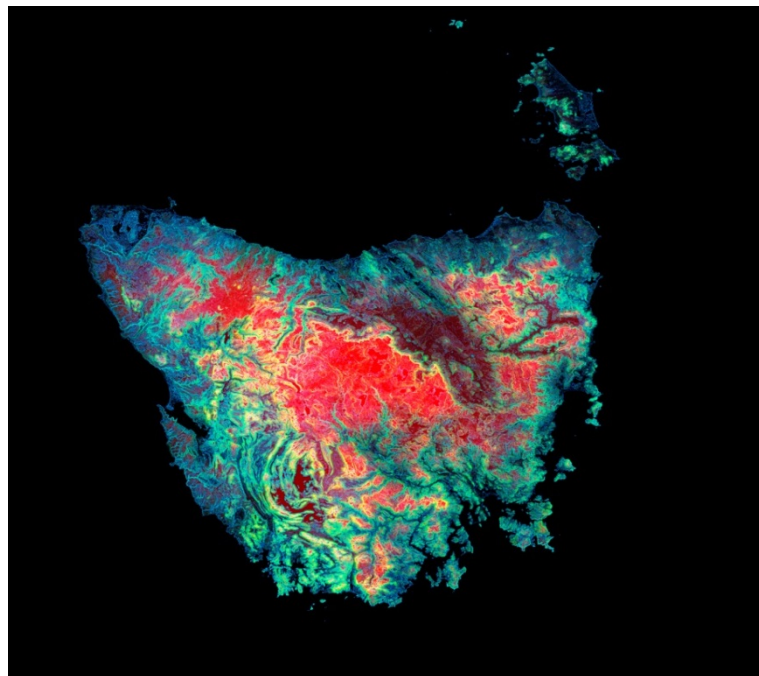


Figure 4.1 Composite of height, slope and curvature for Tasmania

Initial studies showed spikes and serious noise associated with all water covered areas in IDEM data. To avoid this problem, the ocean was set to height zero (above sea level) derived from a SRTM30 based mask. Persistent water bodies on the land were also masked and provided with a height level from SRTM30. The SRTM data height for the water bodies provided a reasonable elevation as fill. However, using these values was simply convenient for processing and did not affect the comparisons as they were excluded from the analysis. However, on the coast and on boundaries of lakes etc. there were still noise areas as the water mask was derived using the criterion that SRTM30 had a slope angle nearly equal to zero in these areas. Therefore the masking did not include some lake and coastal edges which may also have changed due to tides and rainfall. The situation was also exacerbated as the high country areas of Tasmania (including areas glaciated in past periods) have many small lakes and bogs and consequently also have water based noise. In order to ameliorate the remaining effects, a median filter with a threshold was used to remove the worst pits and spikes. The threshold used was more than 15m difference between a 3x3 neighbourhood median and the central value to indicate a severe spike or pit. The pit or spike was replaced by the median value. However, despite these efforts, some serious noise still remained near the edges of lakes and in the littoral zone of all the IDEM data. The total area of elevation data and the mask images provide the final IDEM30 and IDEM12 data bases. There were areas where no IDEM were available. These were included in masks so they could be excluded from comparisons but for convenience of the correction processing they were filled with SRTM30 data or resampled SRTM30 data using cubic convolution where appropriate. SRTM30 data at Landsat multispectral-band scale and resampled SRTM30 data at

Landsat panchromatic scale represent the currently best material available for the purposes of Landsat terrain correction and so have provided a benchmark for the tests.

An image representing terrain altitude, slope and curvature based on IDEM30 data (where it was available), SRTM30 data in the areas of missing IDEM data and masked-out water areas is shown in Figure 4.1. Map registration was initially checked visually using slope and curvature illustrated in Figure 4.1 to identify terrain features (e.g. ridges and drainage) and it was found that these features as well as cultural features remaining in the IDEM data were aligned well with those in the WorldView images used in Google Earth. The enhancements of ridges corresponded to ridges in Google Earth and estimated flow channels aligned closely with rivers. However, as SRTM 90m data are the basis for terrain height in Google Earth, the close match between cultural features remaining in the IDEM data and those in the images used in Google Earth provided more independent validation than just terrain feature matching. These positive statements do, of course, depend on the accurate registration of WorldView images. Google does not publish the registration accuracies of these images but they are generally found to match well with GPS data and are assumed to be accurate to a few pixels (i.e. within 5m). There was certainly no reason for us to suppose other than that SRTM and IDEM data had similar and equally accurate geometry. As found in previous work (Li et al., 2013), the most likely source of mis-registration in the present study will be in the remotely sensed data.

Co-registration and consistency between SRTM30 and IDEM height data was not the primary purpose of this study but was visually assessed using transects across areas with significant terrain relief and mostly clear of water based noise effects. The broad scale (low frequency) features aligned but the IDEM data seemed to have more details than the corresponding SRTM30 data. Mean local altitudes were mostly well aligned so that at the broad trend scale SRTM30 and IDEM30 are consistent DEM models. An example of one such transect is given in Figure 4.2. It is obvious from this and other transects that the IDEM product contains both finer scale information and some additional noise that has been filtered out of the SRTM30 data. Whether the apparent extra detail corresponds to terrain effects in Landsat will be discussed in the following Sections.

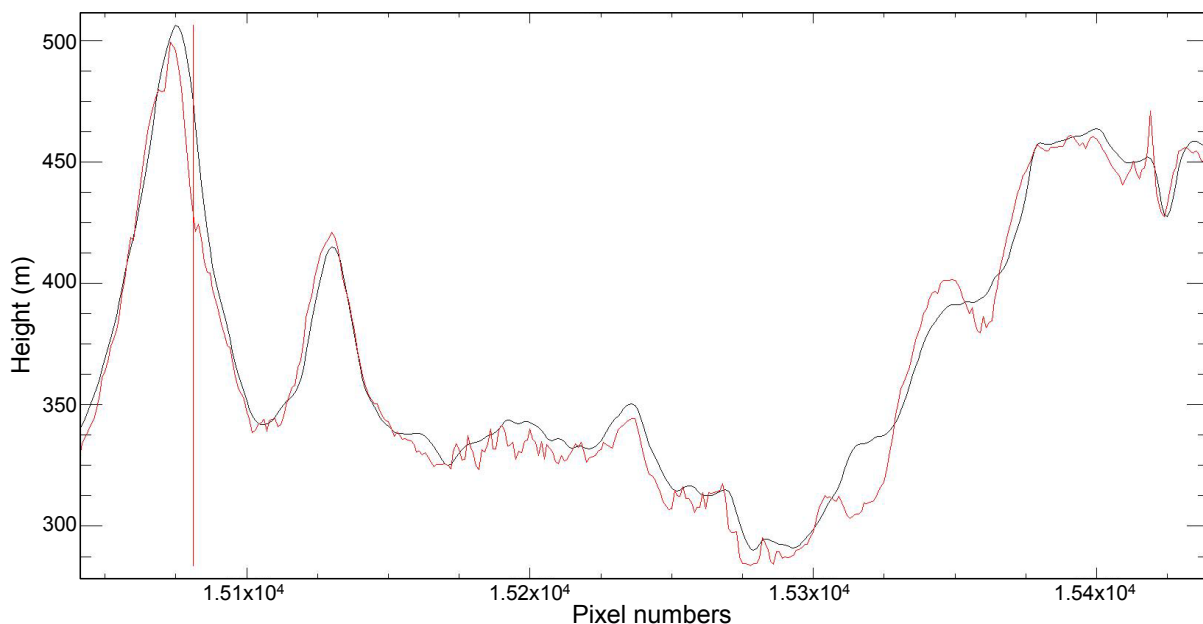


Figure 4.2 Typical horizontal transects from SRTM30 (black) and IDEM30 (red). The vertical red line is the position of the computer cursor on the image display.

4.2 Results from terrain illumination studies

The impact of DEM quality (including their artefacts) and resolution on the terrain correction accuracy was investigated through different processing methods and their comparison. For each DEM data set, the Landsat images were processed into two different products:

1. Standard process (with BRDF and atmospheric correction, but without terrain illumination correction) and
2. Standard process plus terrain illumination correction.

Through the terrain illumination correction, we can visually assess whether terrain shadows are removed efficiently through different DEM data sets and hence detect the relative DEM data quality.

Three DEM data sets were used to process Landsat multispectral bands (bands 2, 3, 4 for Landsat 7 and 3, 4, 5 for Landsat 8). These are the IDEM12, IDEM30 and SRTM30.

Two DSM data sets were used to process Landsat panchromatic band: they are the IDEM12 and SRTM30.

Five different terrain corrected images and two standard images were generated and mosaicked for the whole island of Tasmania. Figure 4.3 is the false colour image (bands 4, 3, 2 for Landsat 7 and 3, 4, 5 for Landsat 8) for Tasmania using IDEM12 data set and Figure 4.10 shows a similar mosaic of the panchromatic bands data.

Since the mosaic images are very large and it is difficult to detect and investigate detailed information, a smaller subset for each path/row has been selected to analyse the results in more detail. Figure 4.4- Figure 4.9 show that much of the terrain shadowing was removed when the topographic correction was applied using the three DEM data sets when compared with the standard processing. However, almost all of the figures show that IDEM12 and IDEM30 are better than the SRTM30 products in some detailed shadowed areas as indicated in areas with fine scale terrain, such as in path 90 and row 90. The difference images also show that surface reflectance could be more than 2 reflectance unit in some areas when different DEM data are used. It is clear in these examples that the products derived using SRTM30 still have residual shadows that are effectively removed in the IDEM12 and IDEM30 derived products.

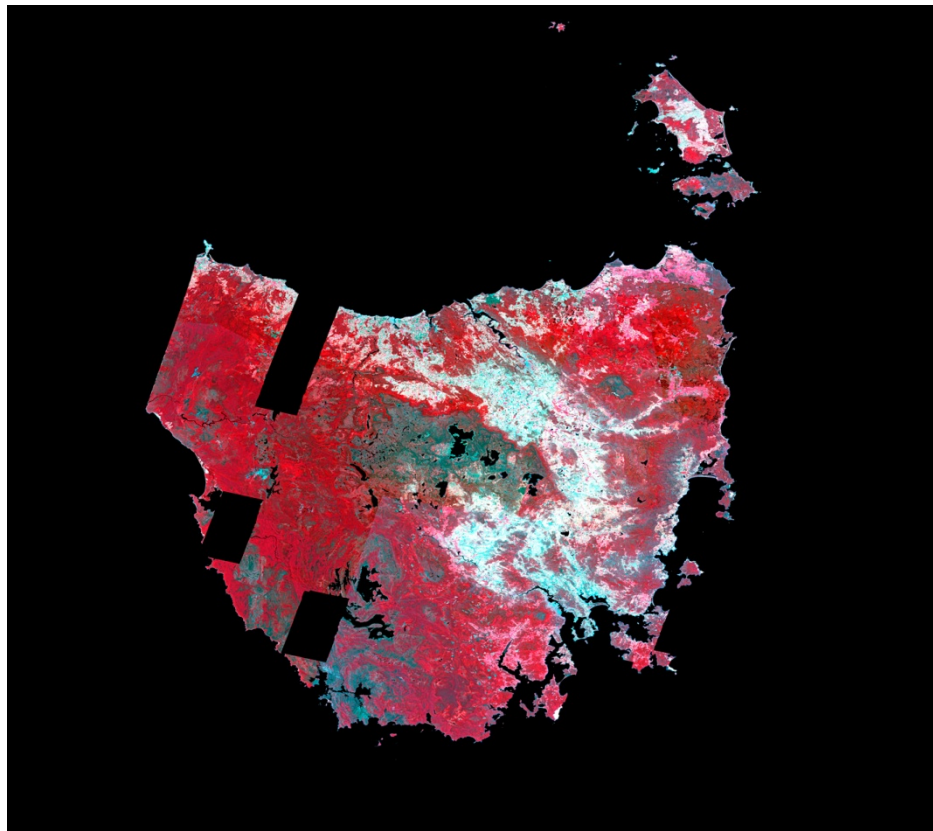


Figure 4.3 Mosaic of terrain corrected Landsat false colour images (bands 4, 3, 2 for Landsat 7 and 5, 4, 3 for Landsat 8) for Tasmania using IDEM 12 m data set

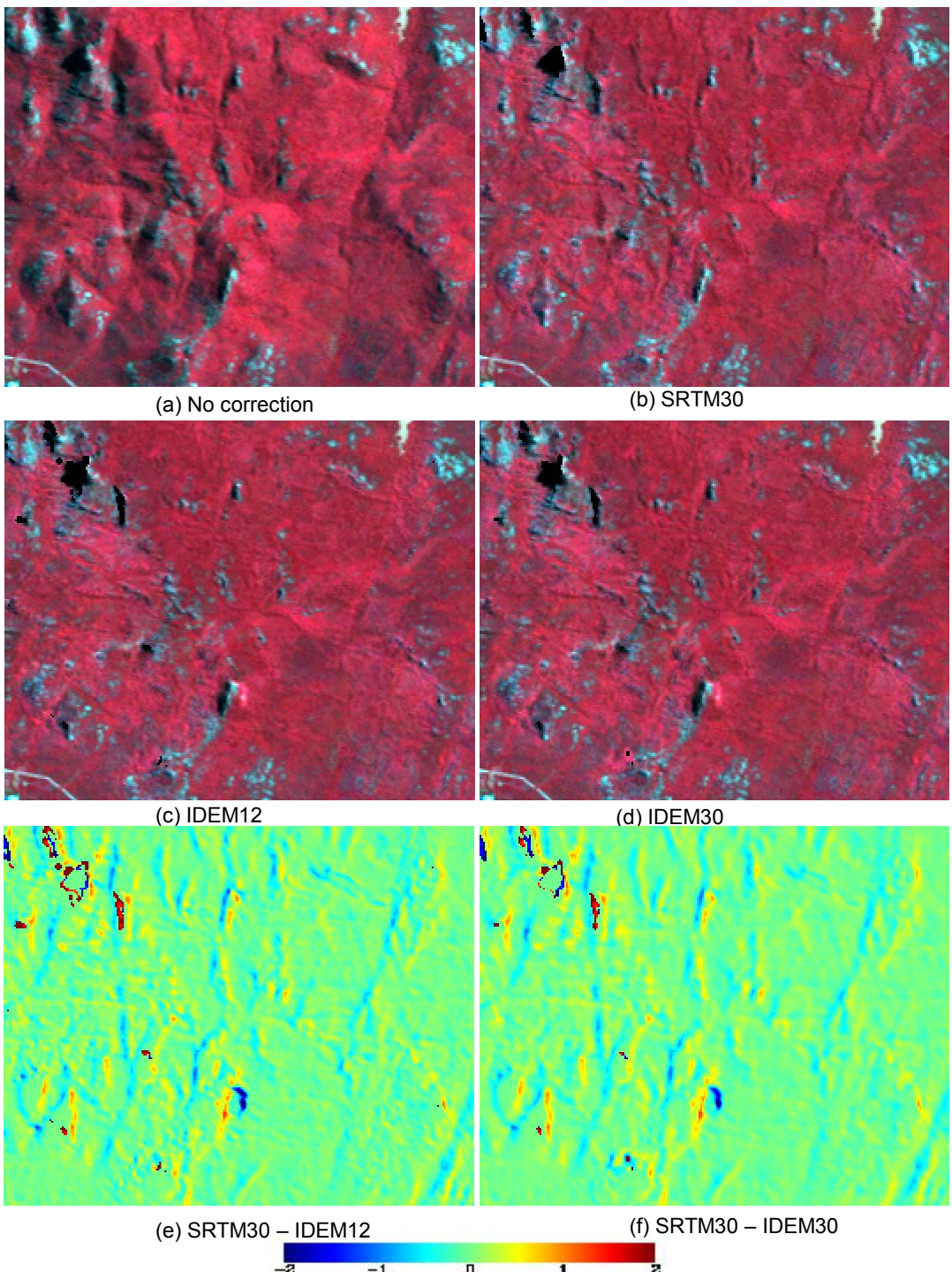


Figure 4.4 False colour image (bands 4, 3, 2) for path 90, row 88 (image 2) using different process methods and DEM data (a) standard method; (b) terrain corrected using SRTM30; (c) terrain corrected using IDEM12 and (d) terrain corrected using IDEM30;. (e) and (f) are the difference images between SRTM30 (b) with IDEM12 (c) and IDEM30 (d) respectively for band 4 in reflectance unit

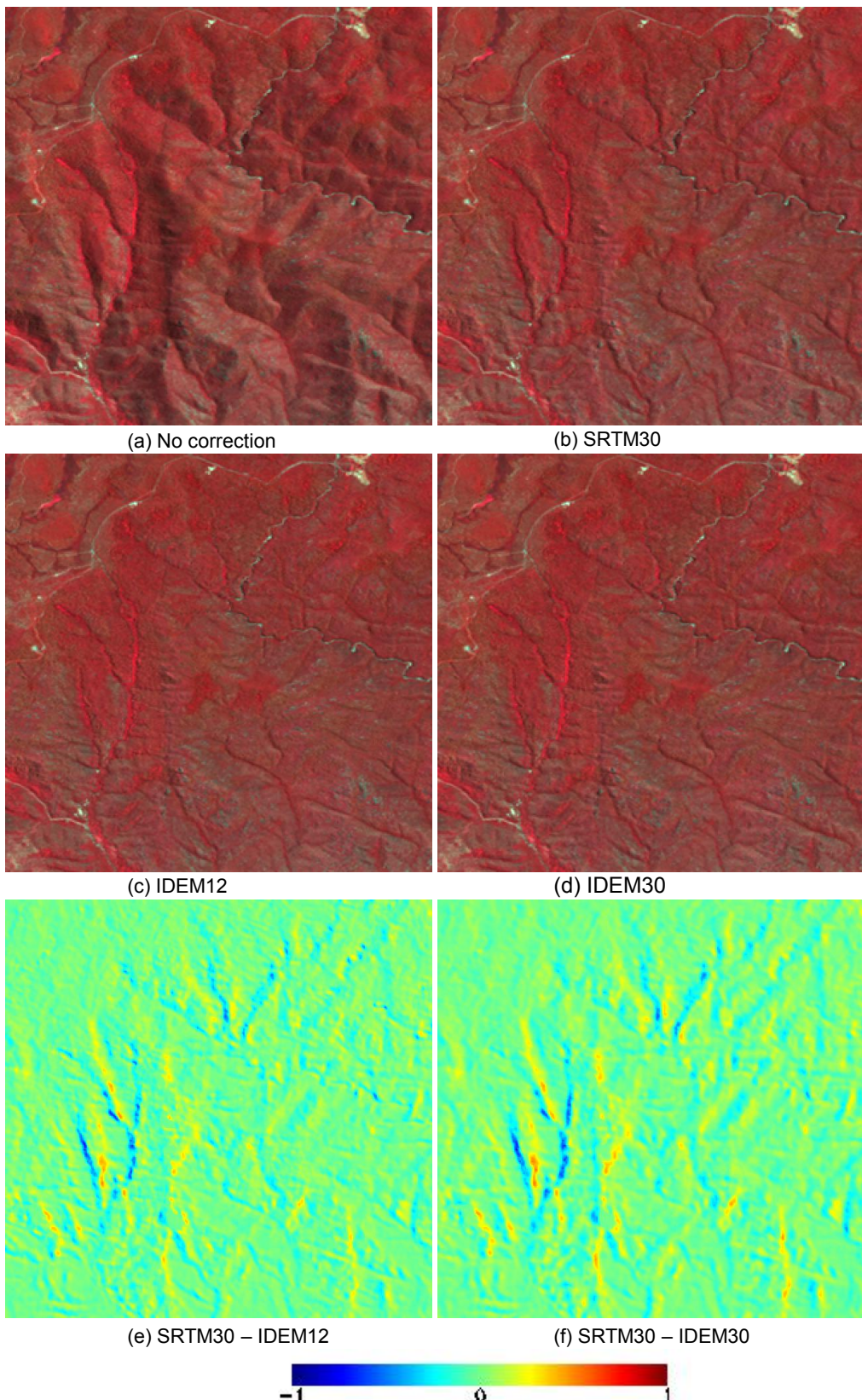


Figure 4.5 False colour image (bands 5, 4, 3) for a subset of path 90, row 89 (image 5) using different process methods and DEM data (a) standard method; (b) terrain corrected using SRTM30; (c) terrain corrected using IDEM12 and (d) terrain corrected using IDEM30; (e) and (f) are the difference images between SRTM30 (b) with IDEM12 (c) and IDEM30 (d) respectively for band 5 in reflectance unit

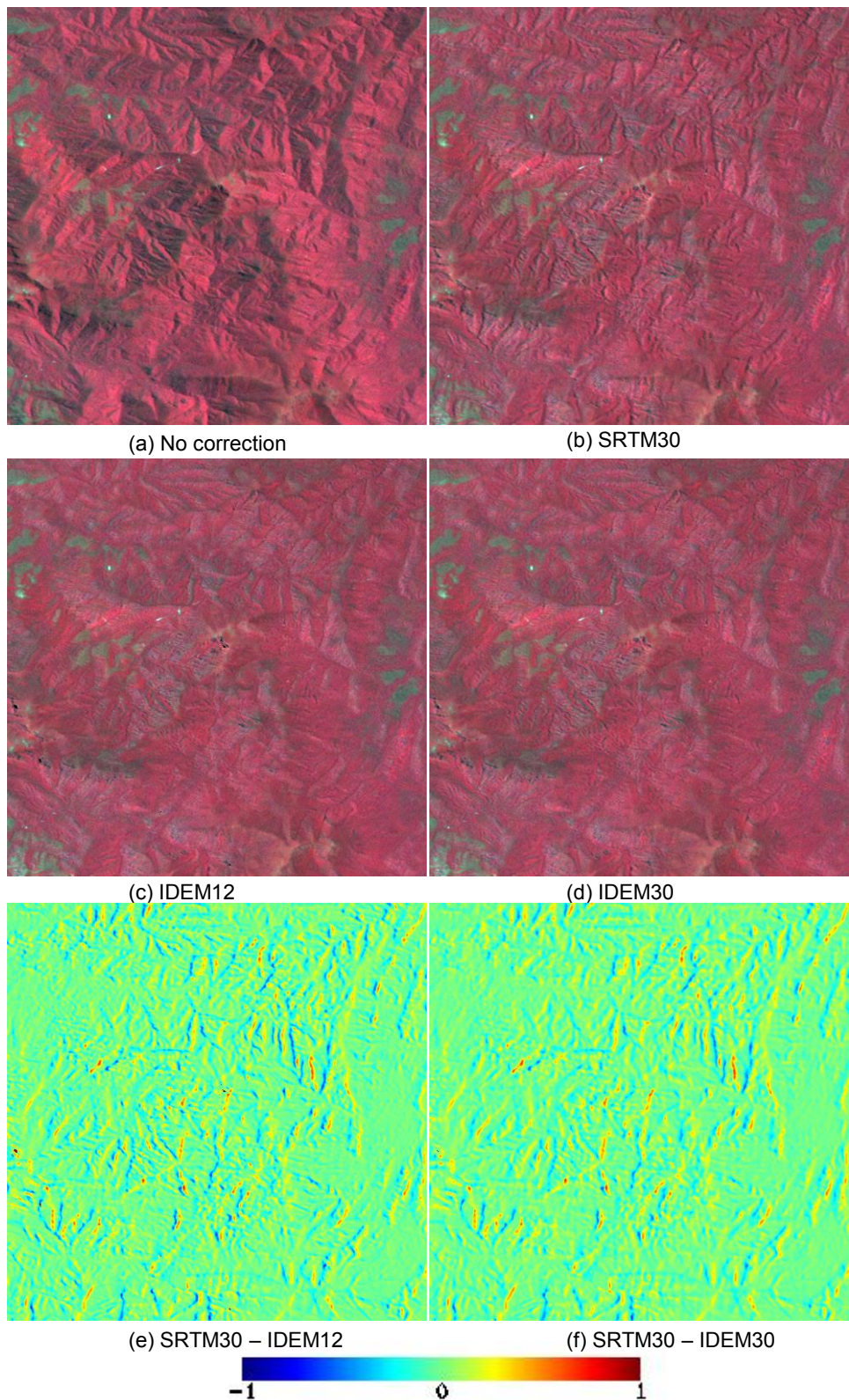


Figure 4.6 False colour image (bands 4, 3, 2) for one subset of path 90, row 90 (image 6) using different process methods and DEM data (a) standard method; (b) terrain corrected using SRTM30; (c) terrain corrected using IDEM12 and (d) terrain corrected using IDEM30; (e) and (f) are the difference images between SRTM30 (b) with IDEM12 (c) and IDEM30 (d) respectively for band 4 in reflectance unit

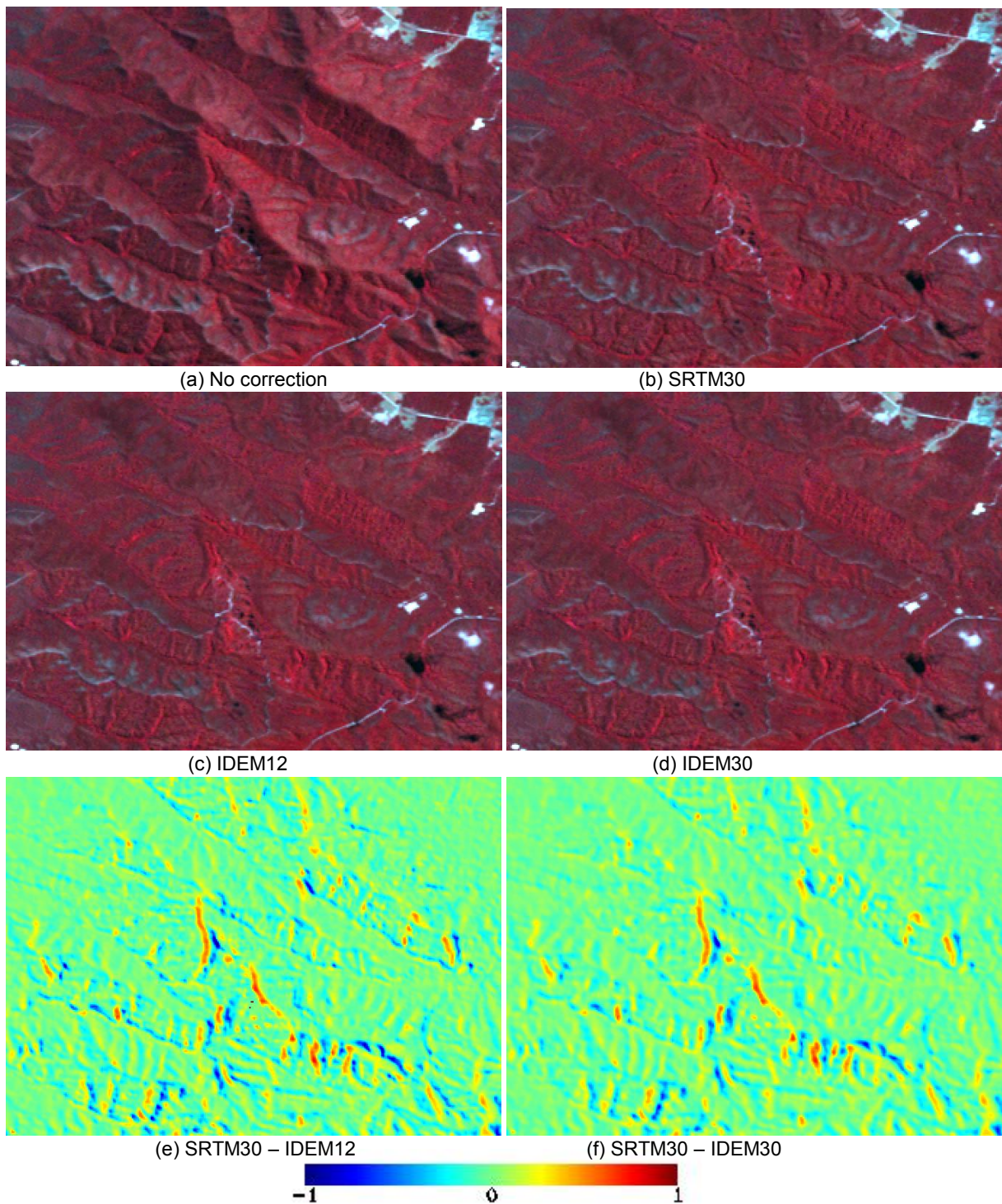


Figure 4.7 False colour image (bands 4, 3, 2) for one subset of path 91, row 88 (image 8) using different process methods and DEM data (a) standard method; (b) terrain corrected using SRTM30; (c) terrain corrected using IDEM12 and (d) terrain corrected using IDEM30; (e) and (f) are the difference images between SRTM30 (b) with IDEM12 (c) and IDEM30 (d) respectively for band 4 in reflectance unit

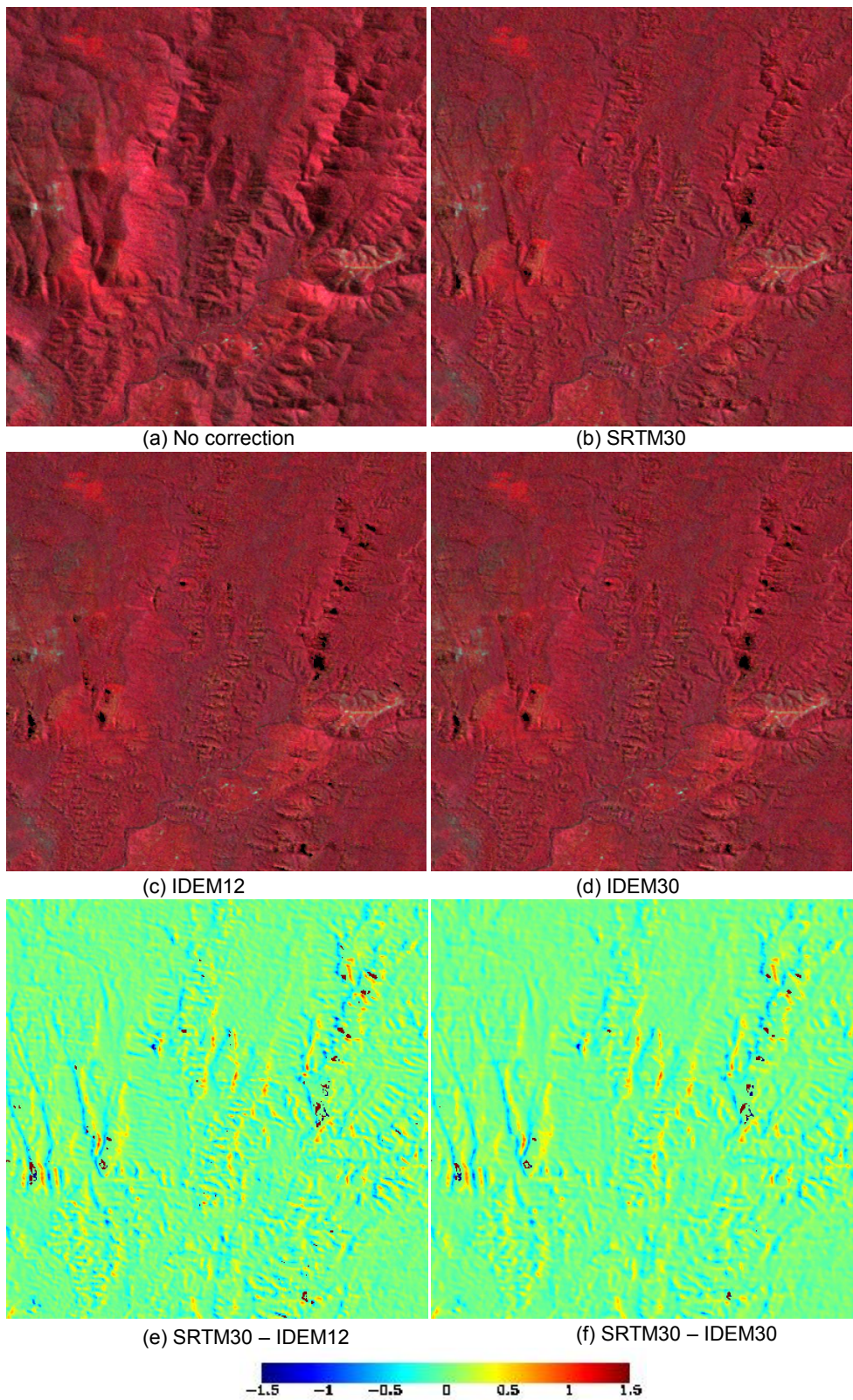


Figure 4.8 False colour image (bands 4, 3, 2) for one subset of path 91, row 89 (image 10) using different process methods and DEM data (a) standard method; (b) terrain corrected using SRTM30; (c) terrain corrected using IDEM12 and (d) terrain corrected using IDEM30; (e) and (f) are the difference images between SRTM30 (b) with IDEM12 (c) and IDEM30 (d) respectively for band 4 in reflectance unit.

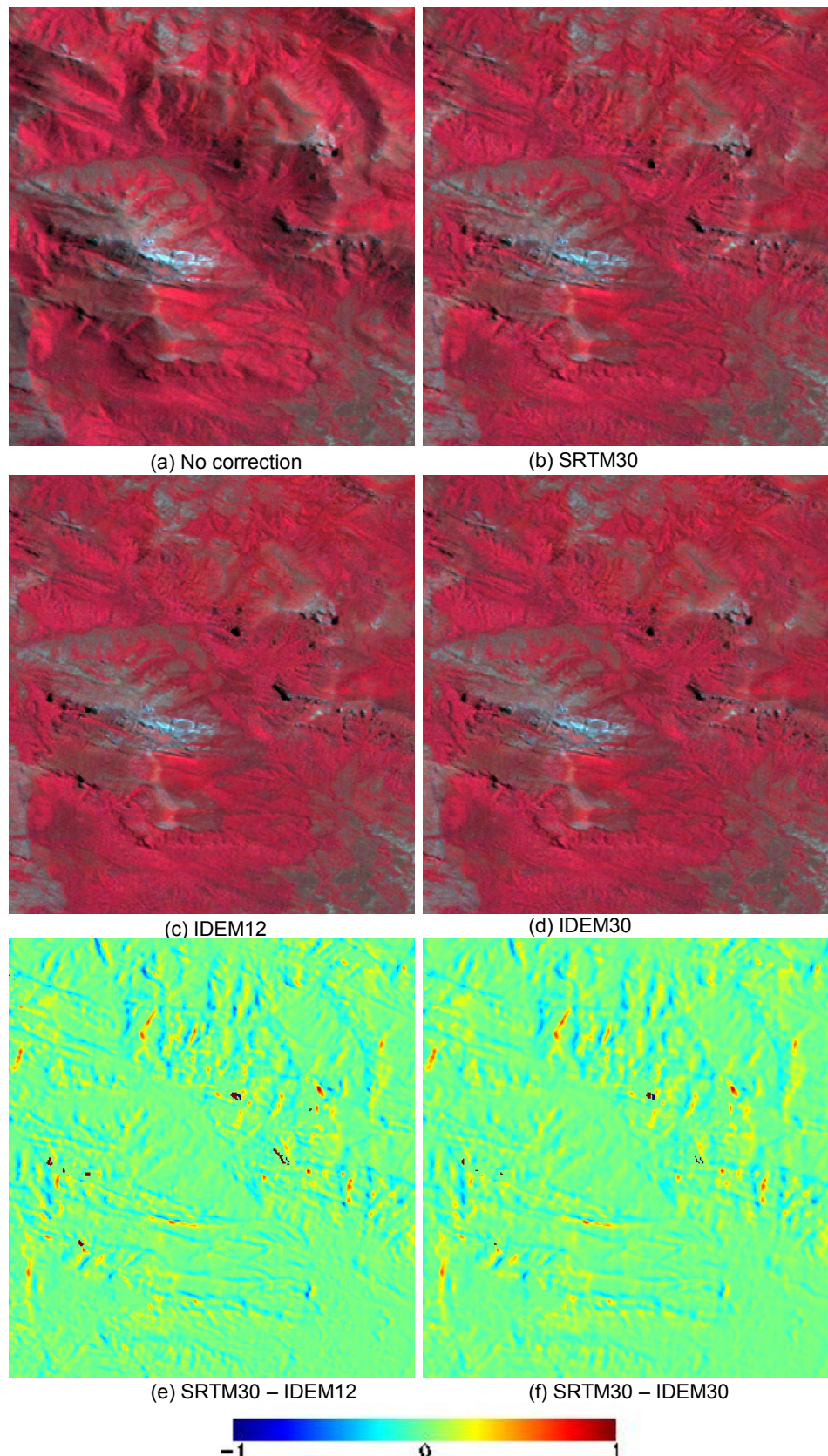


Figure 4.9 False colour image (bands 4, 3, 2) for one subset of path 91, row 90 (image 11) using different process methods and DEM data (a) standard method; (b) terrain corrected using SRTM30; (c) terrain corrected using IDEM12 and (d) terrain corrected using IDEM30; (e) and (f) are the difference images between SRTM30 (b) with IDEM12 (c) and IDEM30 (d) respectively for band 4 in reflectance unit.

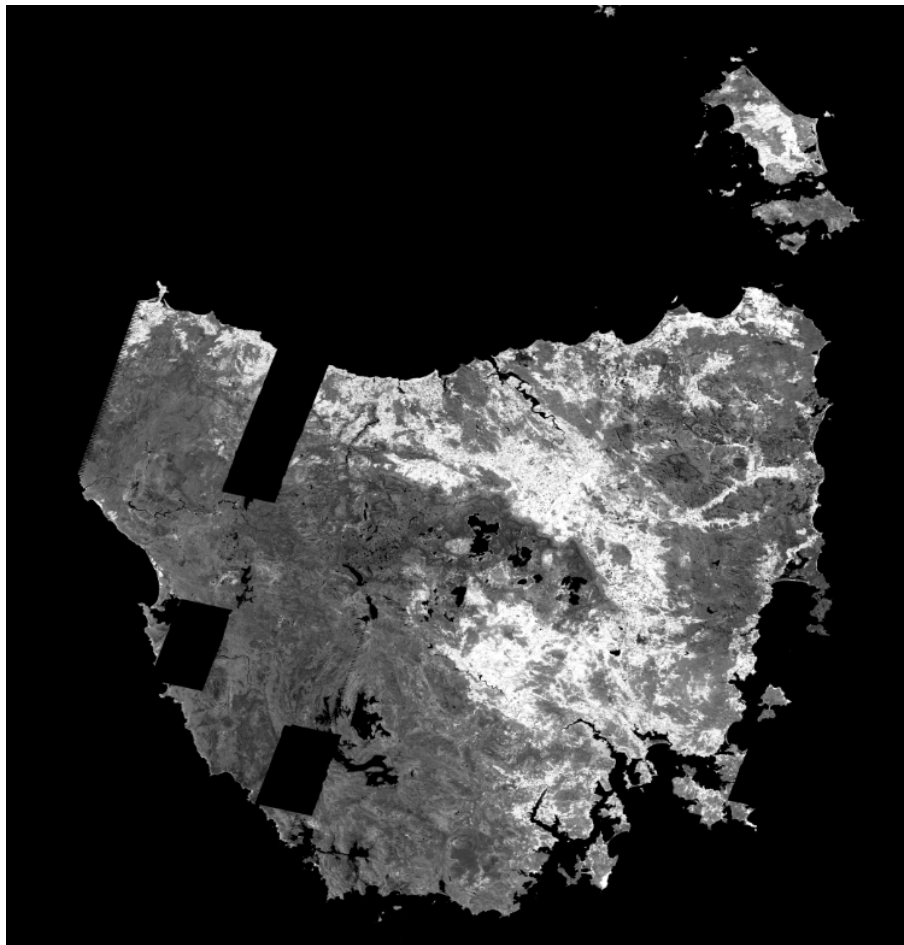


Figure 4.10 Mosaic of terrain corrected Landsat images for Tasmania (band 8) using IDEM12 data set

As with the multispectral bands situation, the panchromatic mosaic image is too large to detect and investigate detailed information. Therefore, the same smaller subsets as for the multispectral bands for each path/row have been used to visually assess the results. The equivalent situations are illustrated in Figure 4.11-Figure 4.16. The findings are similar to those from the false colour of multispectral bands in that the IDEM12 produces better results in the areas with small scale of terrain. Many shadows caused by fine scale structures in areas with small scale terrain are removed. However, Figure 4.11 and Figure 4.14 also show that IDEM12 seems to have some uncorrelated noise when it is used to process at the resolution of band 8 (0.45 arc sec).

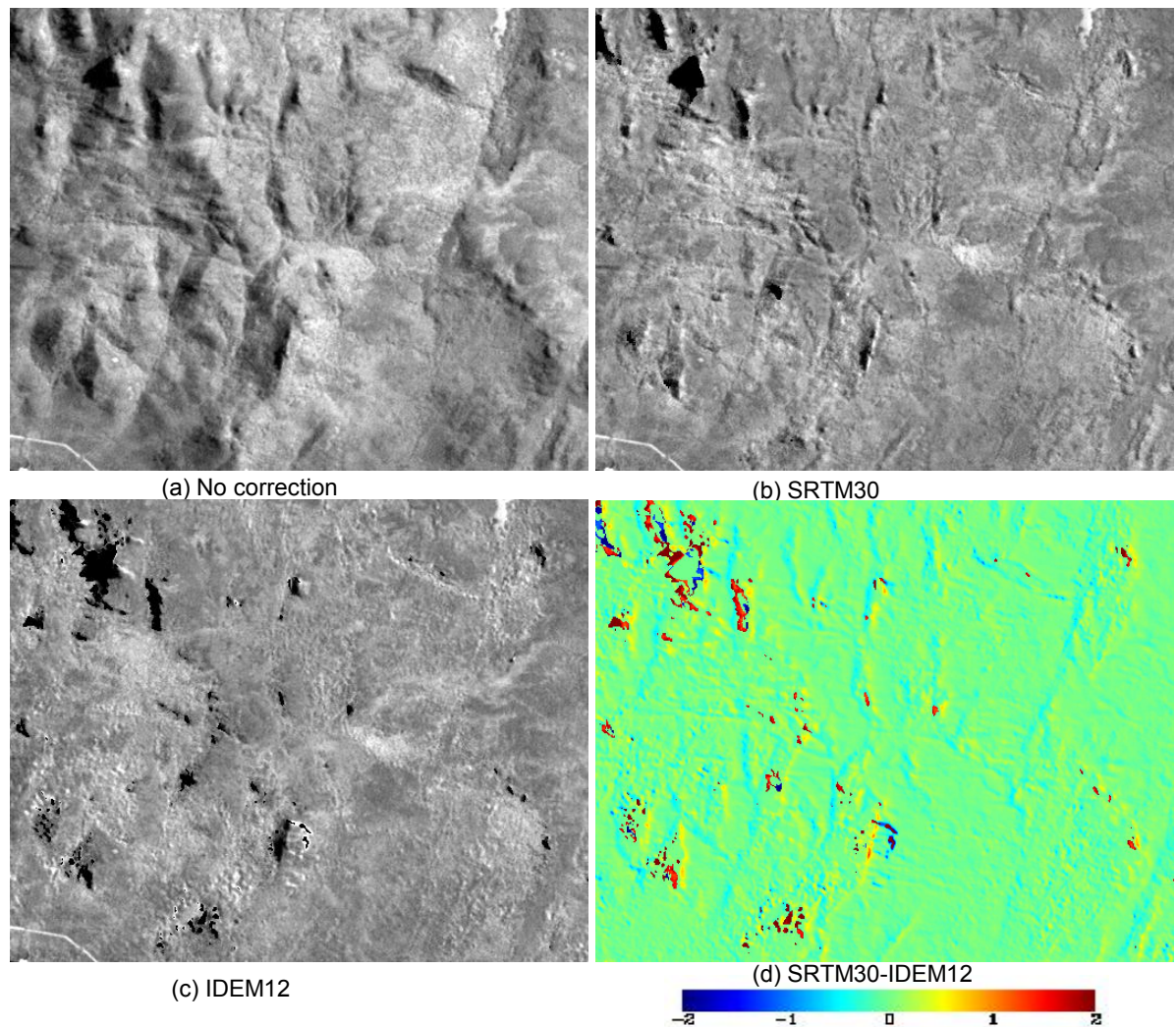


Figure 4.11 A subset of band 8 for path 90, row 88 (image 2) using different process methods and DEM data (a) standard method; (b) terrain corrected using SRTM30; (c) terrain corrected using IDEM12 and (d) difference between SRTM30 (b) and IDEM12 (c)

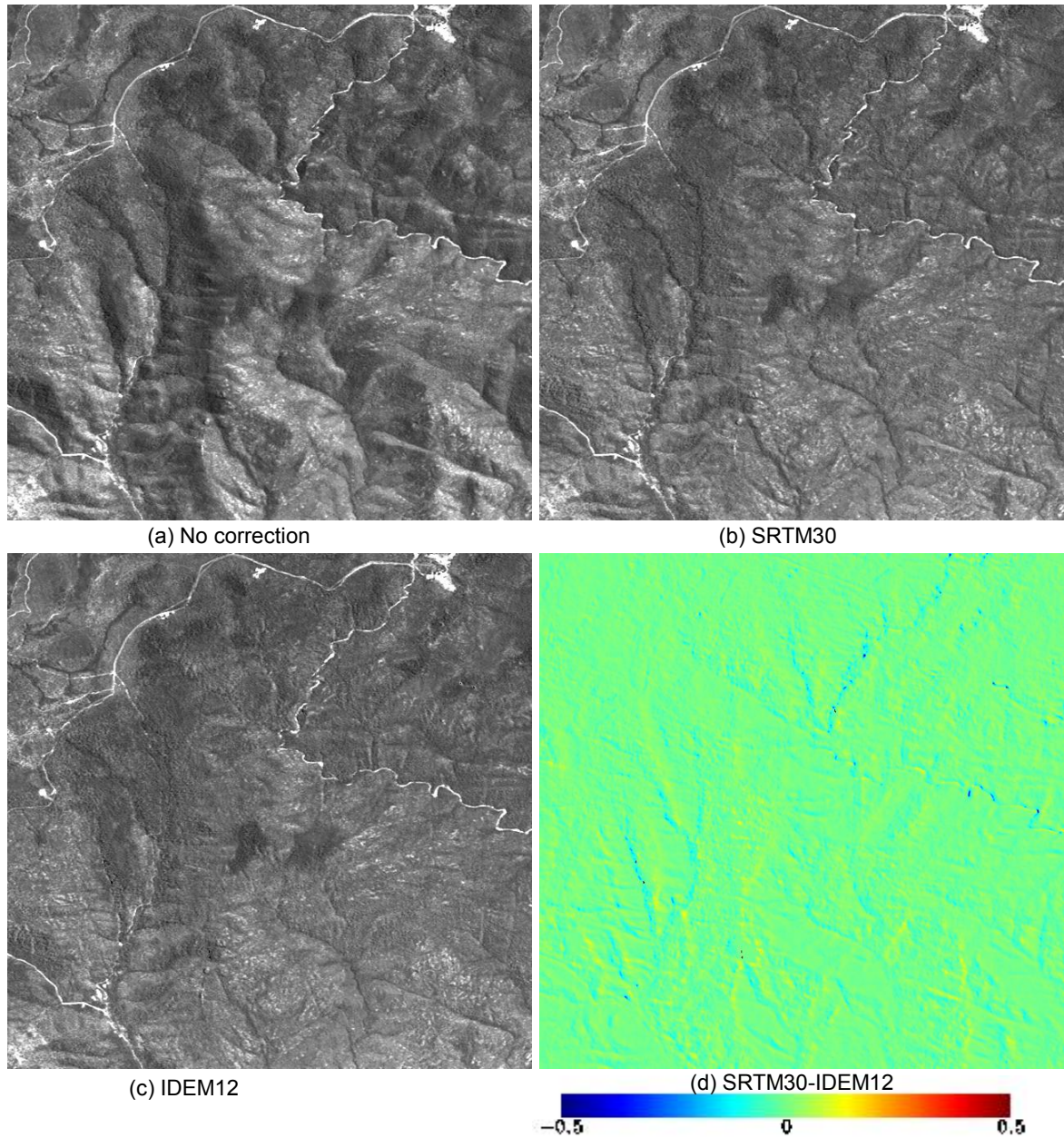


Figure 4.12 A subset of band 8 for path 90, row 89 (image 5) using different process methods and DEM data (a) standard method; (b) terrain corrected using SRTM30; (c) terrain corrected using IDEM12 and (d) difference between SRTM30 (b) and IDEM12 (c)

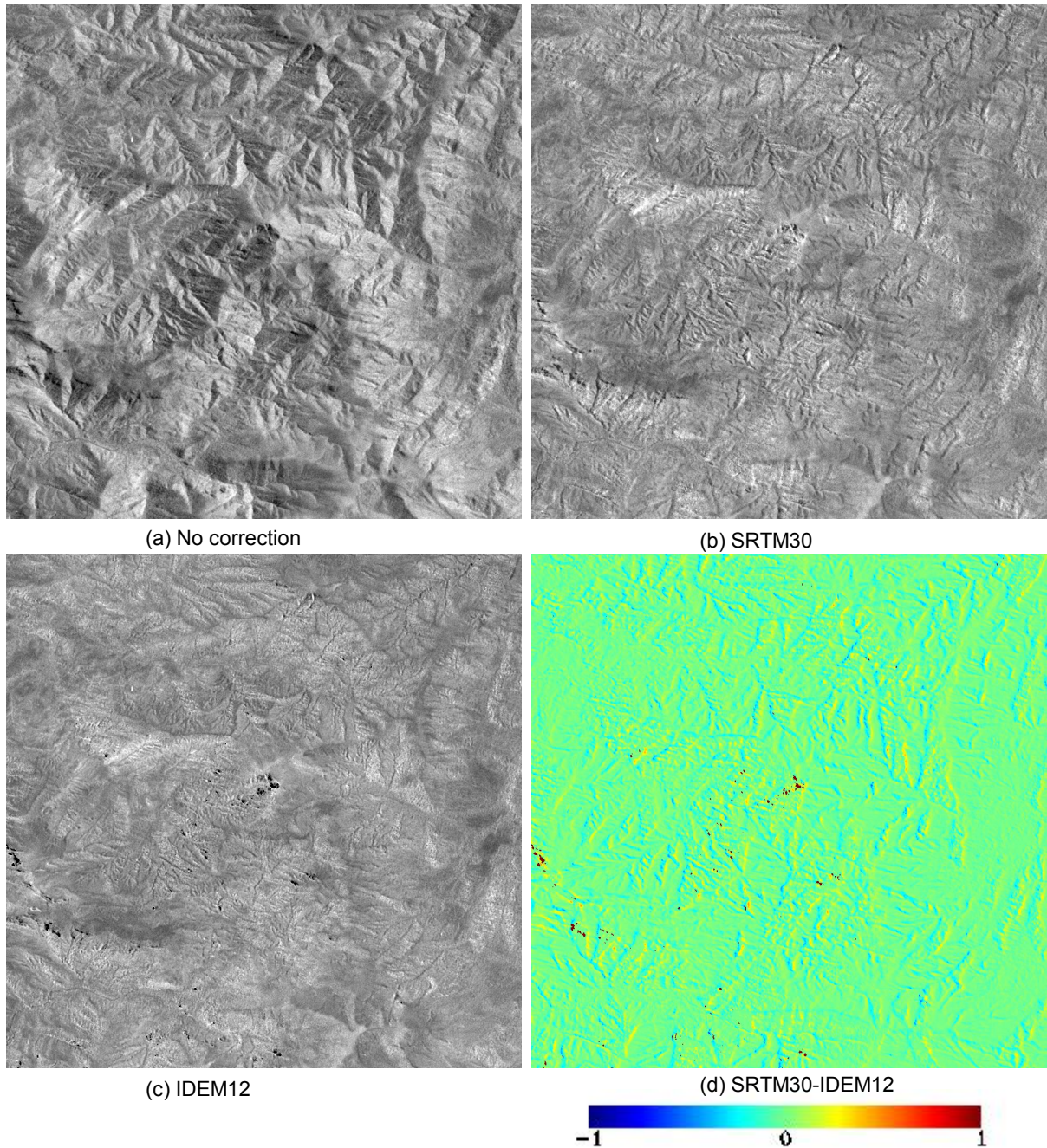


Figure 4.13 A subset of band 8 for path 90, row 90 (image 6) using different process methods and DEM data (a) standard method; (b) terrain corrected using SRTM30; (c) terrain corrected using IDEM12 and (d) difference between SRTM30 (b) and IDEM12 (c).

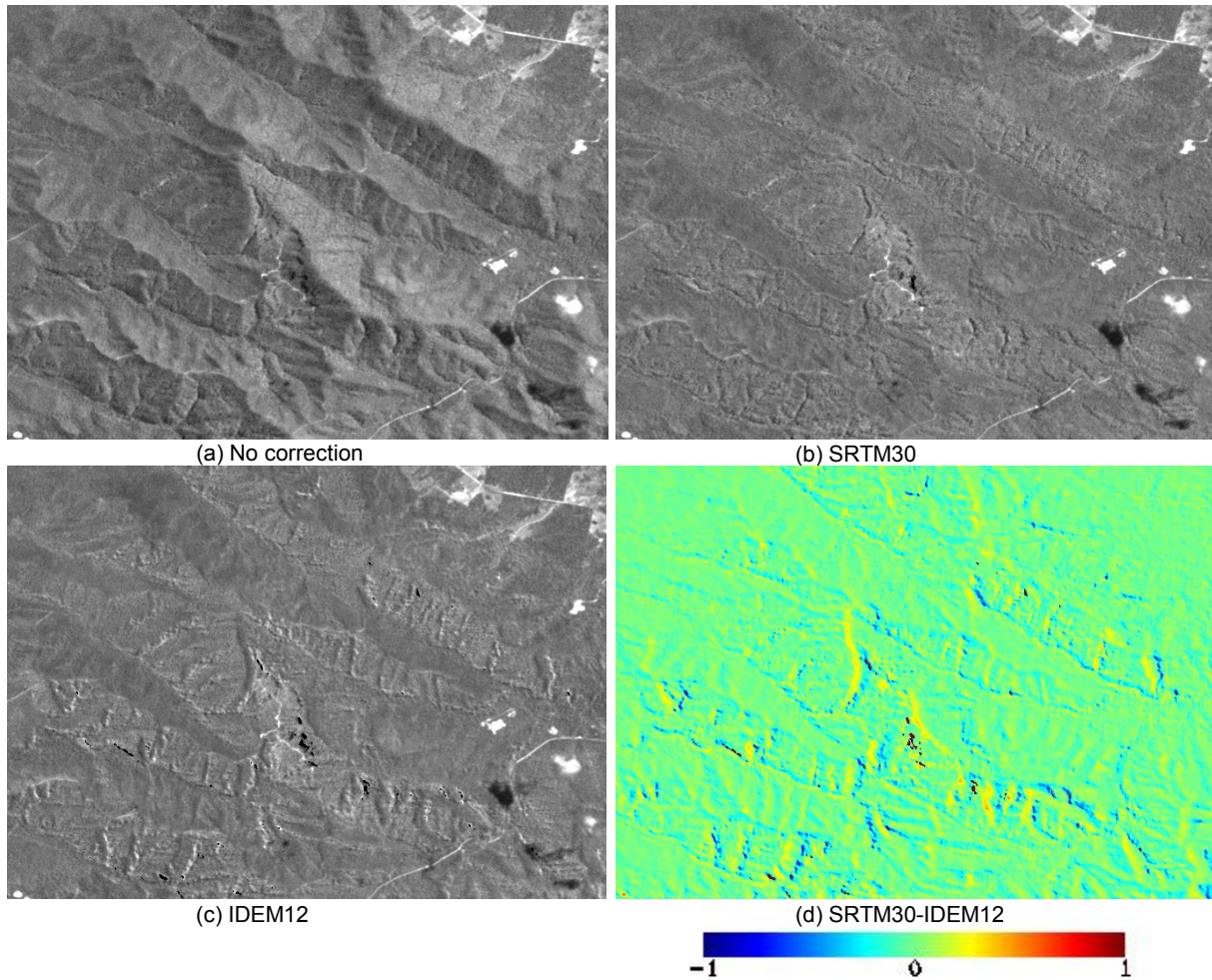


Figure 4.14 A subset of band 8 for path 91, row 88 (image 8) using different process methods and DEM data (a) standard method; (b) terrain corrected using SRTM30; (c) terrain corrected using IDEM12 and (d) difference between SRTM30 (b) and IDEM12 (c)

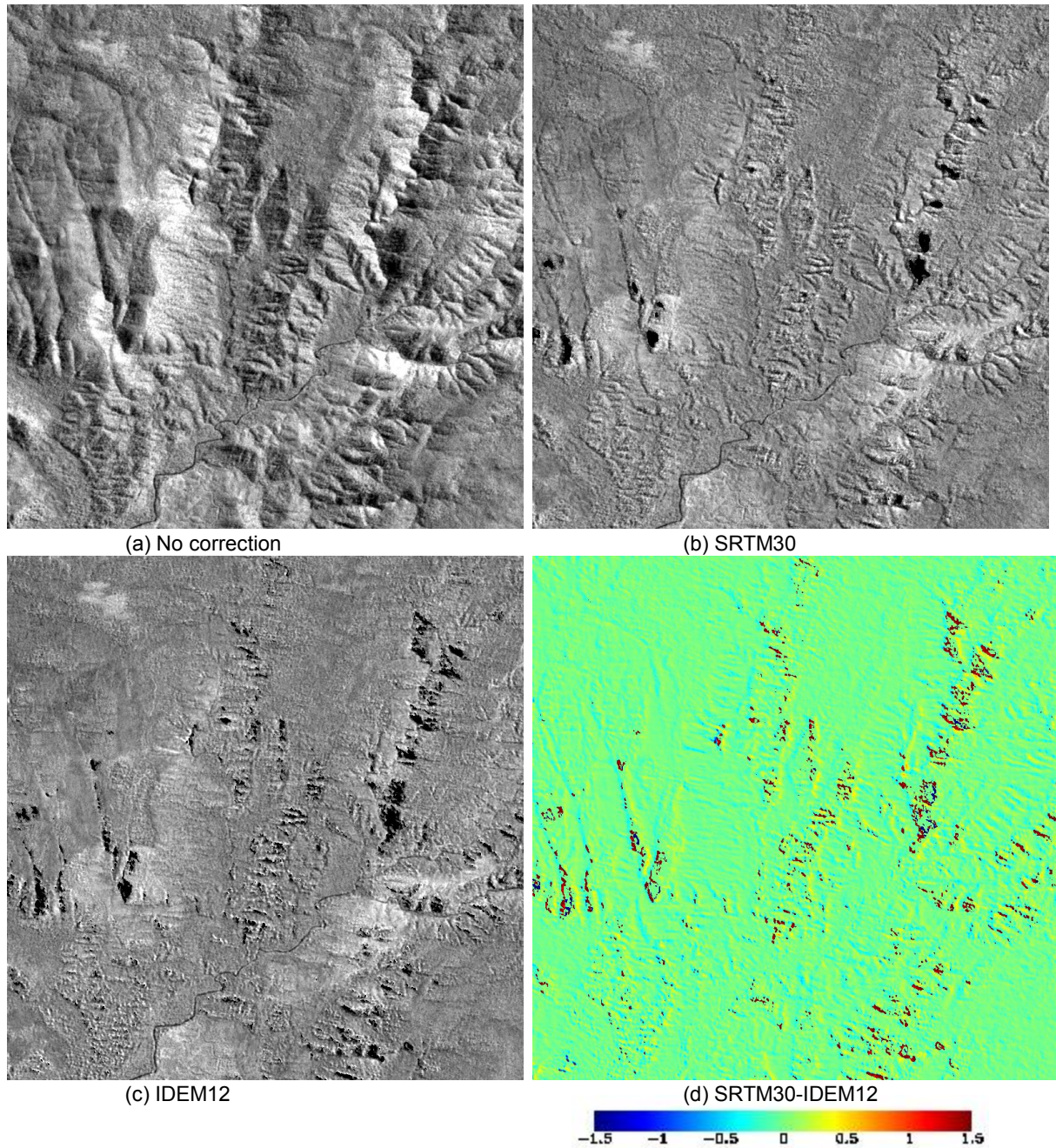


Figure 4.15 A subset of band 8 for path 91, row 89 (image 10) using different process methods and DEM data (a) standard method; (b) terrain corrected using SRTM30; (c) terrain corrected using IDEM12 and (d) difference between SRTM30 (b) and IDEM12 (c)

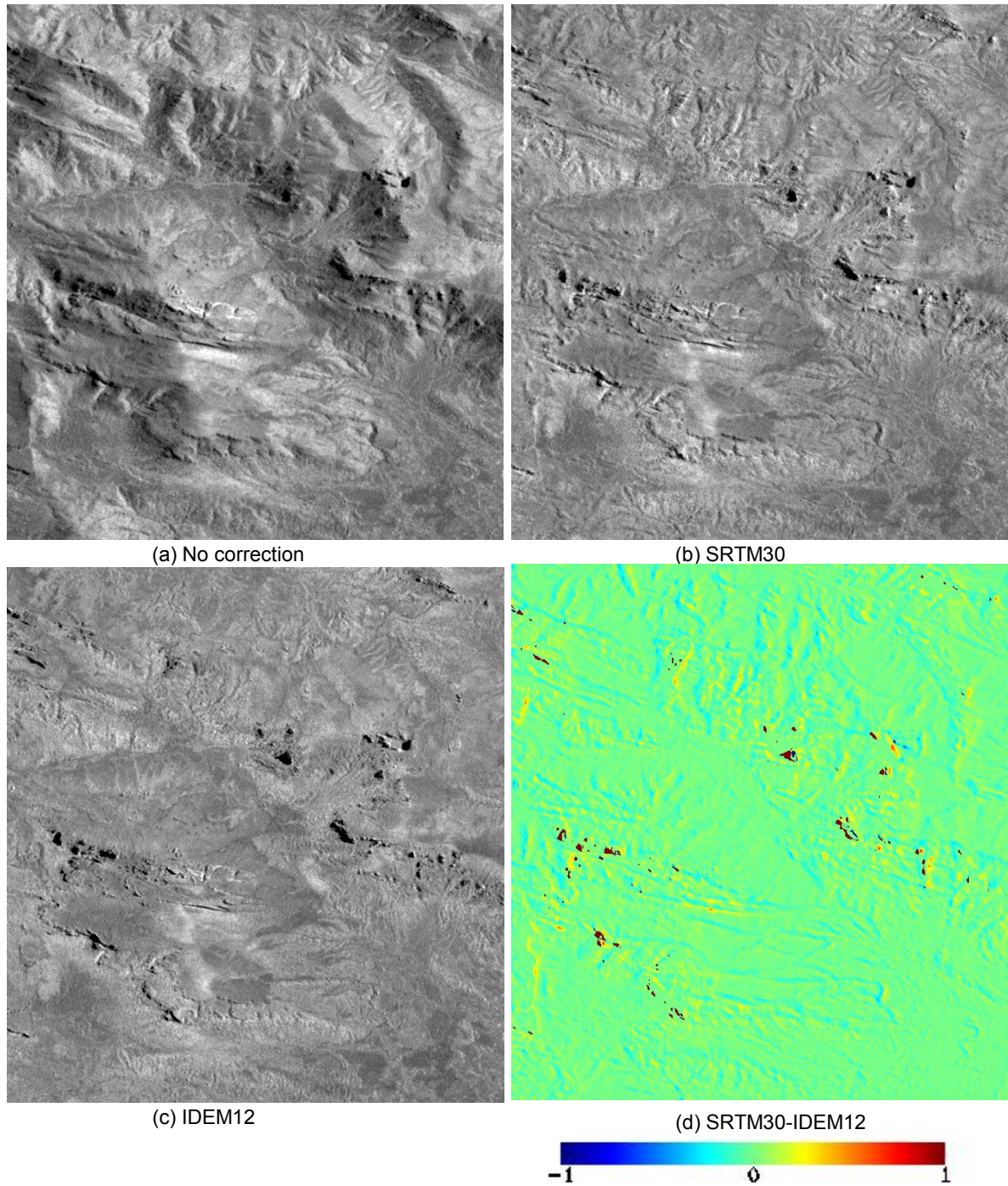


Figure 4.16 A subset of band 8 for path 91, row 90 (image 11) using different process methods and DEM data (a) standard method; (b) terrain corrected using SRTM30; (c) terrain corrected using IDEM12; and (d) difference between SRTM30 (b) and IDEM12 (c)

Correlation coefficient between cosine incident angle and the four different products in the near-infrared (NIR) band (band 4 for Landsat 7 and band 5 for Landsat 8) and three different products in band 8 are listed in Table 4.1 and Table 4.2 respectively. The results show that IDEM12 in general has high correlation reductions and SRTM30 has the lowest correlation reduction. However, high negative correlation in Table 4.2 shows that mis-registration and noise are occurring between band 8 and the IDEM12. The source of these effects will need further investigation but it seems that both data sets are contributing.

Table 4.1 Correlation coefficients of subsets for each Landsat image of NIR band and its corresponding cosine incident angle

| Image number | IDEM12 | | IDEM30 | | SRTM30 | |
|--------------|--------|---------|--------|---------|--------|---------|
| | before | after | before | after | before | after |
| 1 | 0.6804 | 0.0287 | 0.6766 | 0.0363 | 0.7148 | 0.1103 |
| 2 | 0.8269 | 0.1187 | 0.8229 | 0.1434 | 0.8378 | 0.1978 |
| 3 | 0.7447 | -0.1822 | 0.7447 | -0.1571 | 0.7536 | -0.1250 |
| 4 | 0.9274 | -0.1198 | 0.9215 | -0.0641 | 0.9128 | 0.0062 |
| 5 | 0.8299 | 0.0020 | 0.8138 | 0.0052 | 0.7841 | -0.0093 |
| 6 | 0.8218 | -0.1249 | 0.8171 | -0.0753 | 0.7570 | -0.1017 |
| 7 | 0.8408 | -0.1240 | 0.8382 | -0.0632 | 0.7832 | -0.0864 |
| 9 | 0.8032 | 0.0699 | 0.7929 | 0.0975 | 0.7549 | 0.0678 |
| 10 | 0.8396 | 0.1792 | 0.8258 | 0.2024 | 0.7874 | 0.1701 |
| 11 | 0.8056 | -0.0351 | 0.8026 | -0.0105 | 0.7754 | -0.0313 |
| 12 | 0.8341 | -0.1650 | 0.8320 | -0.1315 | 0.8017 | -0.1471 |

Table 4.2 Correlation coefficients of subsets for each Landsat image of band 8 and its corresponding cosine incident angle

| Image number | IDEM12 | | SRTM30 | |
|--------------|--------|---------|--------|---------|
| | before | after | before | after |
| 1 | 0.5994 | -0.1749 | 0.6498 | -0.0898 |
| 2 | 0.7845 | -0.1517 | 0.8157 | -0.0008 |
| 3 | 0.7035 | -0.1714 | 0.6939 | -0.1122 |
| 4 | 0.8908 | -0.1390 | 0.8858 | 0.0223 |
| 5 | 0.5783 | 0.0688 | 0.5733 | 0.0931 |
| 6 | 0.8019 | -0.3430 | 0.7371 | -0.2405 |
| 7 | 0.8194 | -0.2255 | 0.7644 | -0.1150 |
| 9 | 0.7562 | -0.0697 | 0.7350 | 0.0399 |
| 10 | 0.7817 | -0.0284 | 0.7580 | 0.1096 |
| 11 | 0.8370 | -0.0767 | 0.7892 | -0.0601 |
| 12 | 0.8575 | -0.1792 | 0.8166 | -0.1220 |

4.3 Results from Filter Bank analysis

The filter bank method is an extension of an often used way to model terrain shading. That is, to correlate the cosine of the incident radiation (cosit) with the Landsat data in areas that are mountainous and with small variations in land cover type and condition. In the empirical method, a linear regression is used to correct the shading but this has been replaced now by physical methods in most cases. Because the model based only on the cosine of incident radiation correlation (cosit) assumes little or no diffuse radiation, the correlation is often established for near-infrared (NIR) and shortwave infrared (SWIR) bands or (sometimes) a principal component composite band etc. For example, Figure 4.17(a) and Figure 4.17(b) show (respectively) a mountainous area in our study area with primarily forest cover in the NIR band of a Landsat image (a) and its cosine of incident angle (b).

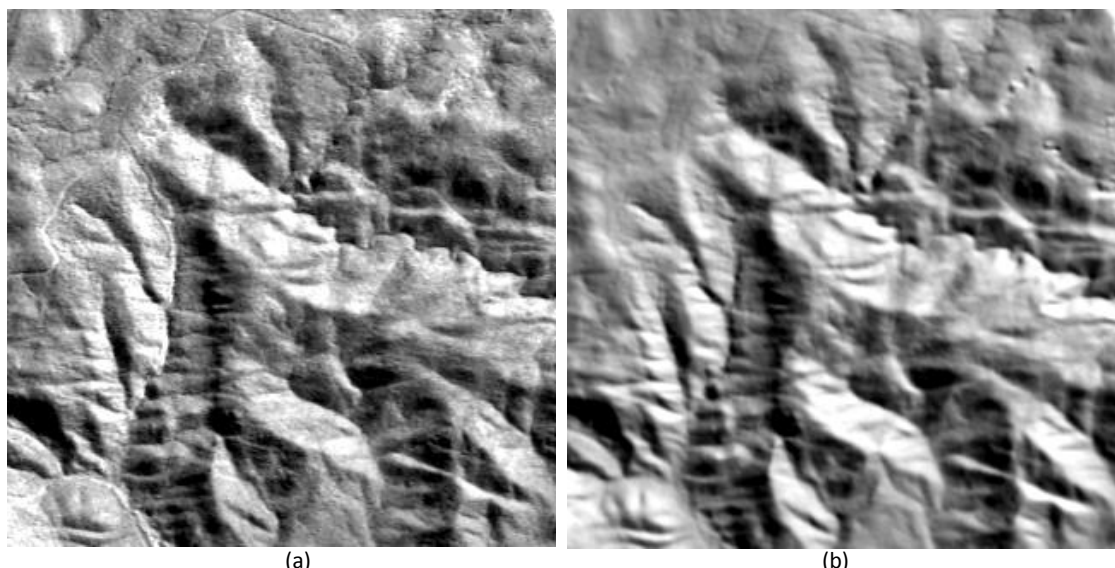


Figure 4.17 Area of forested mountains and (b) cosine of incident angle for the given sun angle based on slope and aspect from a DEM (in this case the IDEM12 data aggregated to Landsat resolution).

The goodness of fit between the data sets can be expressed as a correlation. The relationship will be stronger when there is significant variation in the cosit function. This occurs for areas of high relief and for a given area when the sun elevation is lower. As noted, it is also better for NIR (band 4 for Landsat 7 and band 5 for Landsat 8) or SWIR spectral bands. From experiments undertaken, it has been difficult to obtain such test areas for the Tasmanian region. One reason is the frequent cloud cover. Another is that land covers can change in condition over time and between seasons – especially the condition of the alpine grasslands and change in the size of water bodies in the lacustrine area between summer (hot and dry) and winter (wet and cool). But with care, a set of geographic regions was found that were clear of disturbances and they have been used as targets to visually assess the results of terrain correction.

For example, a Landsat 8 image has been studied among the images used in Tasmania. Its overall two-way relationship with the corresponding cosit function for the NIR band and panchromatic band (cosit based in each case on IDEM12) over the corresponding test area can be visualised in Figure 4.18.

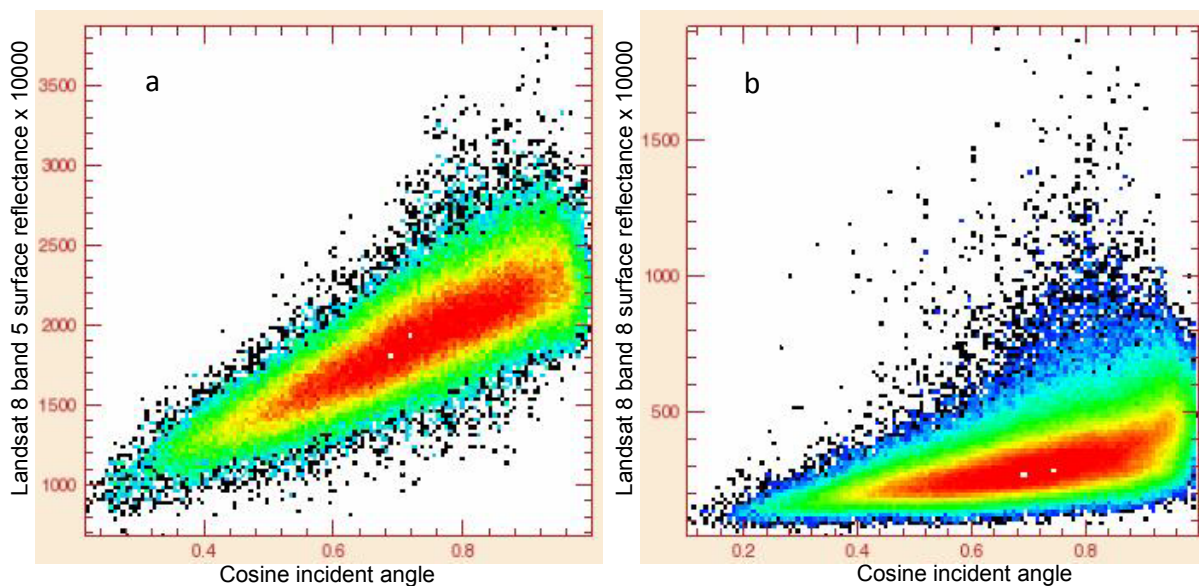


Figure 4.18 XY density plot between surface reflectance and cosine incident angle: (a) band 5 and (b) band 8

There is clearly an overall high correlation between the two images and it occurs for all choices of DEM and the resulting overall correlations are listed in Table 4.1 and Table 4.2. However, this overall plot does not indicate where geographically the correlation arises in the data. DEMs have resolutions defined by the size of the grid cell or pixel making up the basic elements of the DEM. They also have "scale" which will here be taken as the highest spatial frequencies accurately represented in the data. Fine scale is indicated by many details in the data that are missing from coarse scale data. Resolution, of course, defines the upper limit for this. Li et al. (2013) provides some examples of different scales associated with SRTM 30m (1 arc second) and 90m (3 arc seconds) data sampled at the same resolution. The 90m data are deficient in details that are present in the 30m data. The question is therefore how well they correlate in detail rather than in the overall trend.

The level of correlation between scale components of a DEM is measured by the filter bank. Basically, the filters split the Landsat data and the cosine incident angle function into frequency components and establish how the correlations change with the split. If one DEM has a finer scale than another but is no finer than Landsat then it will have more components correlated with the cosit at higher frequencies than the other. The effects on the image correlation can be illustrated by plotting the same data as in Figure 4.18 but after application of the filter to Landsat data and to the corresponding cosit function. This is shown for different filters in Figure 4.19.

The filter with $kf=21$ only removes broad trends from the data and the correlations are not very different from those of the original data. For $kf=11$, the band 5 data still show clearly correlated behaviour but the band 8 has become nearly uncorrelated with the $kf=11$ filter. We can clarify this behaviour by following the change in correlation with filter bank width and for various combinations of DEM by plotting the various cases as will be illustrated below. To do this we have labelled the five uses of the DEMs available as follows. The labels are:

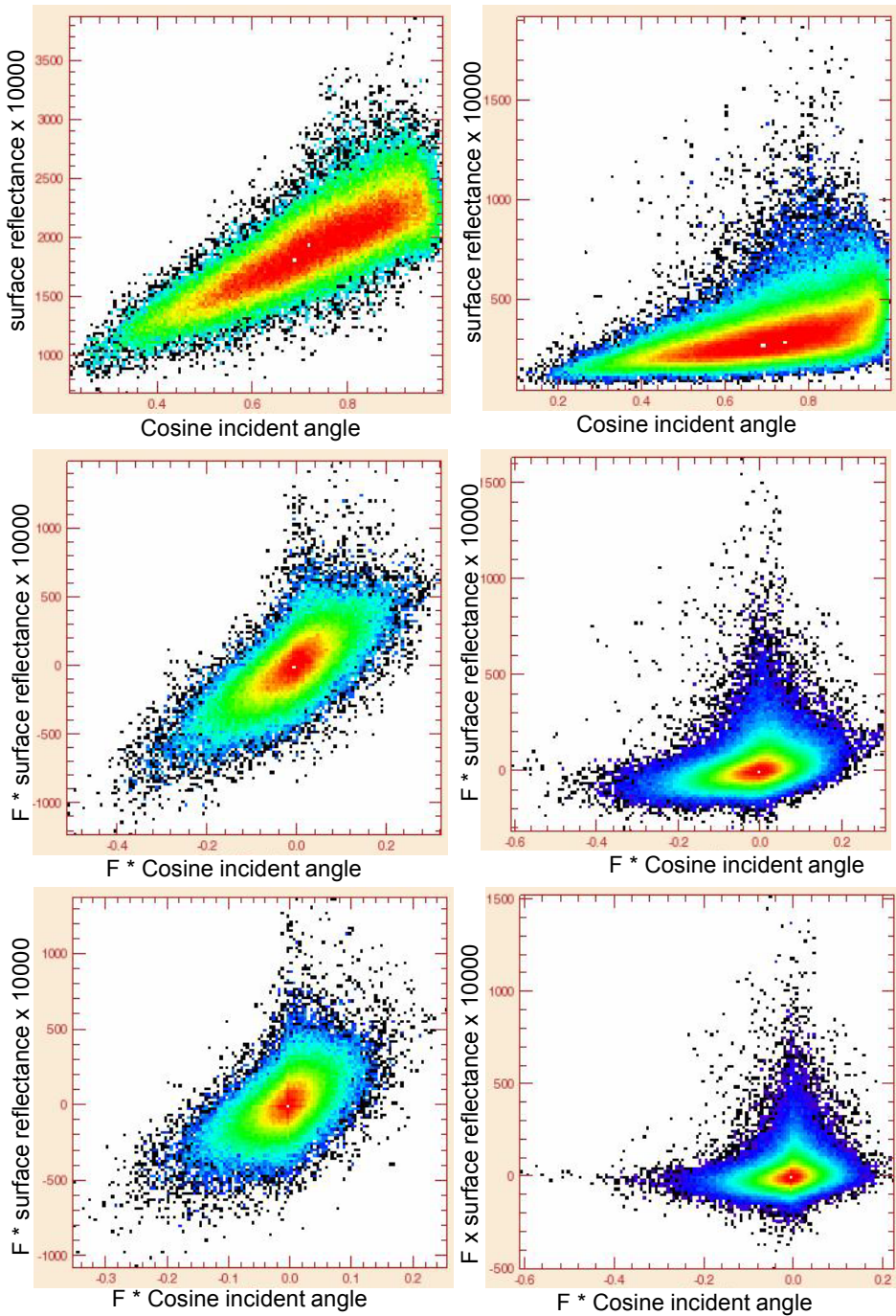


Figure 4.19 Left hand column is Landsat 8 band 5 data; from top to bottom is the base data, a filter with $kf=21$ for both Landsat and DEM data and a filter with $kf=11$ for Landsat and DEM data; the right hand column is the same for the band 8 data. F in the figure means filter has been applied to the data.

DEM1 – SRTM30 data at Landsat multispectral bands resolution

DEM2 – IDEM30 data at Landsat multispectral bands resolution

DEM3 – IDEM12 aggregated to Landsat multispectral bands resolution

DEM4 – SRTM30 resampled to Landsat panchromatic band resolution by cubic convolution

DEM5 – IDEM12 data at Landsat panchromatic band resolution

Each of these defines a cosit function. For the Landsat data used in Figure 4.20 we can show set of scale related plots, for the multispectral band data (the NIR band which has less diffuse radiation than visible bands) (Figure 4.20):

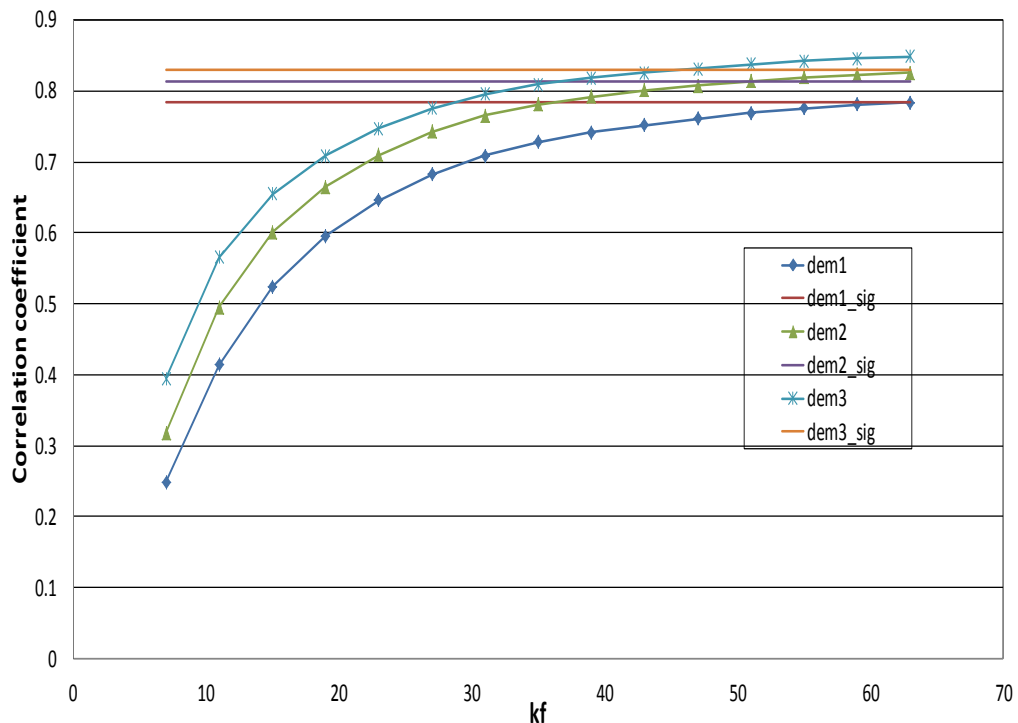


Figure 4.20 Correlation coefficient changes with function of the high pass filter width kf for band 5

Figure 4.20 plots the correlation between the Landsat data and the cosit function as a function of the width of the applied filter. Small values of kf indicate images where only the highest frequencies of the data are remaining. The unfiltered image correlations (listed in Table 4.1 and Table 4.2) are plotted for reference and denoted by “sig”. Due to the decreasing signal to noise ratio as kf reduces, the correlation falls. However, DEM3, the DEM where IDEM12 data aggregated to Landsat multispectral bands resolution, persists with higher correlations than any other. Figure 4.21 show the case of the band 8.

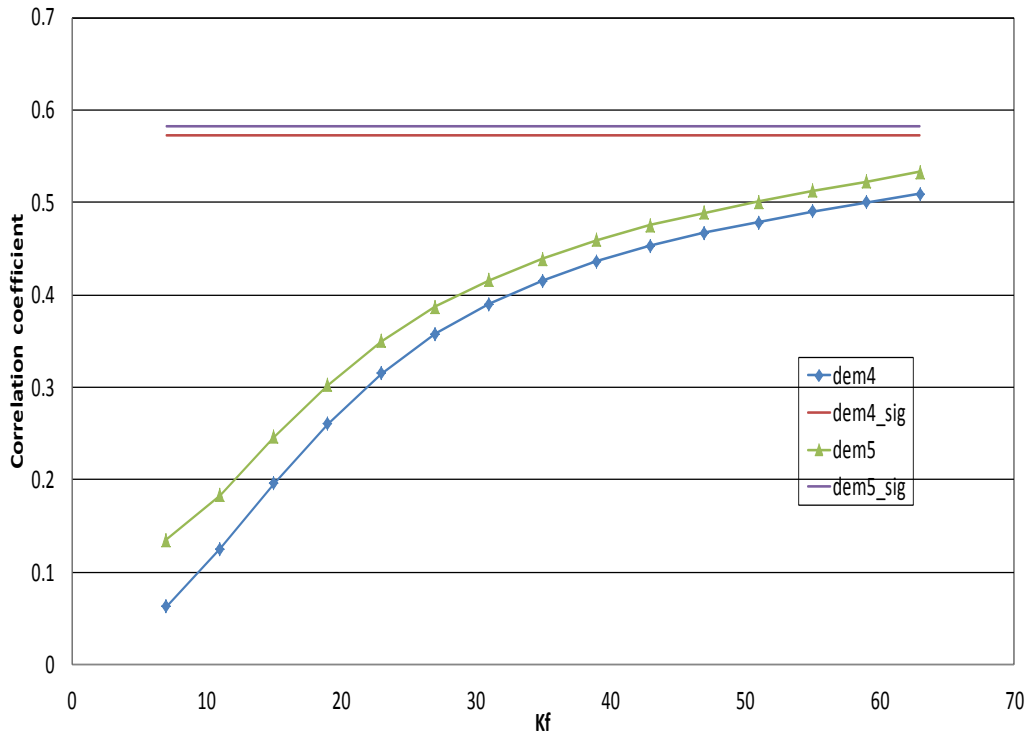


Figure 4.21 Correlation coefficient changes with function of the high pass filter width kf for band 8

The correlations of both the resampled SRTM30 and the IDEM12 based data reduce quickly as kf decreases (low frequencies are removed), with the IDEM12 apparently having marginally more details that correlate with details in the Landsat data. But the difference is small and it seems possible than neither the DEMs nor the Landsat data have a lot of correlated information at the finest scales that can be represented in the panchromatic data.

The data have been studied in this way over all of the subsets chosen, but for this report they are summarised by overall correlations in Table 4.1 and Table 4.2, it is sufficient to note in summary that the above behaviour is common to the areas with high variance of the cosit function. They support the visually assessed conclusions that the IDEM based data generally have more detailed terrain features than the corresponding SRTM data and overall, they provide useful improvement. The correlation analysis cannot identify specific places in the images where details are picked up by one method or another.

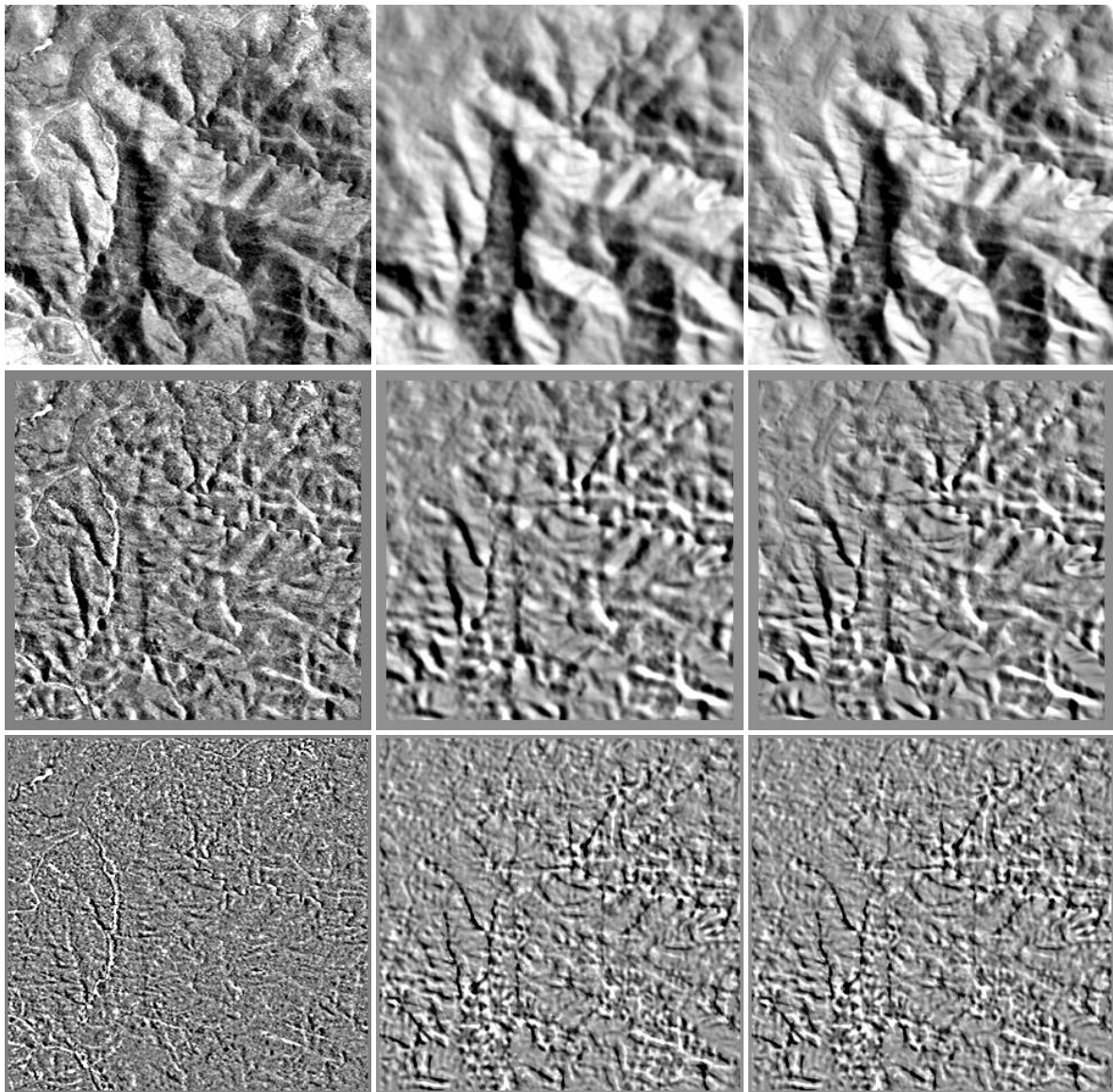


Figure 4.22 Landsat band 5 (left column), cosit from SRTM30 (middle column) and cosit from IDEM12 (right column) for unfiltered (top row), filtered with $kf = 19$ (middle row) and filtered with $kf = 11$ (bottom row).

Another way to understand the effects of scale is to directly view the images of filtered data. For the same Landsat 8 data, we can illustrate this approach as follows (Figure 4.22).

As expected from the plots shown above and the general results summarised in Table 4.1 and Table 4.2, both DEMs show a high level of correlation with the Landsat data. The row 3 suggests the Landsat data is losing spatial details before either DEM. Which DEM is “best” seems to rest with which one can remove the finest detail terrain components which visual evidence provided above suggests is the IDEM data. Statistically, they are all useful DEMs.

The second Table of images (Figure 4.23) is arranged in a similar way to the first but its image data are panchromatic data and the DEMs compared are DEM4 and DEM5. Again as suggested by the plots of correlation with scale, information seems to be lost almost completely at the finest resolutions – in this case $kf=11$.

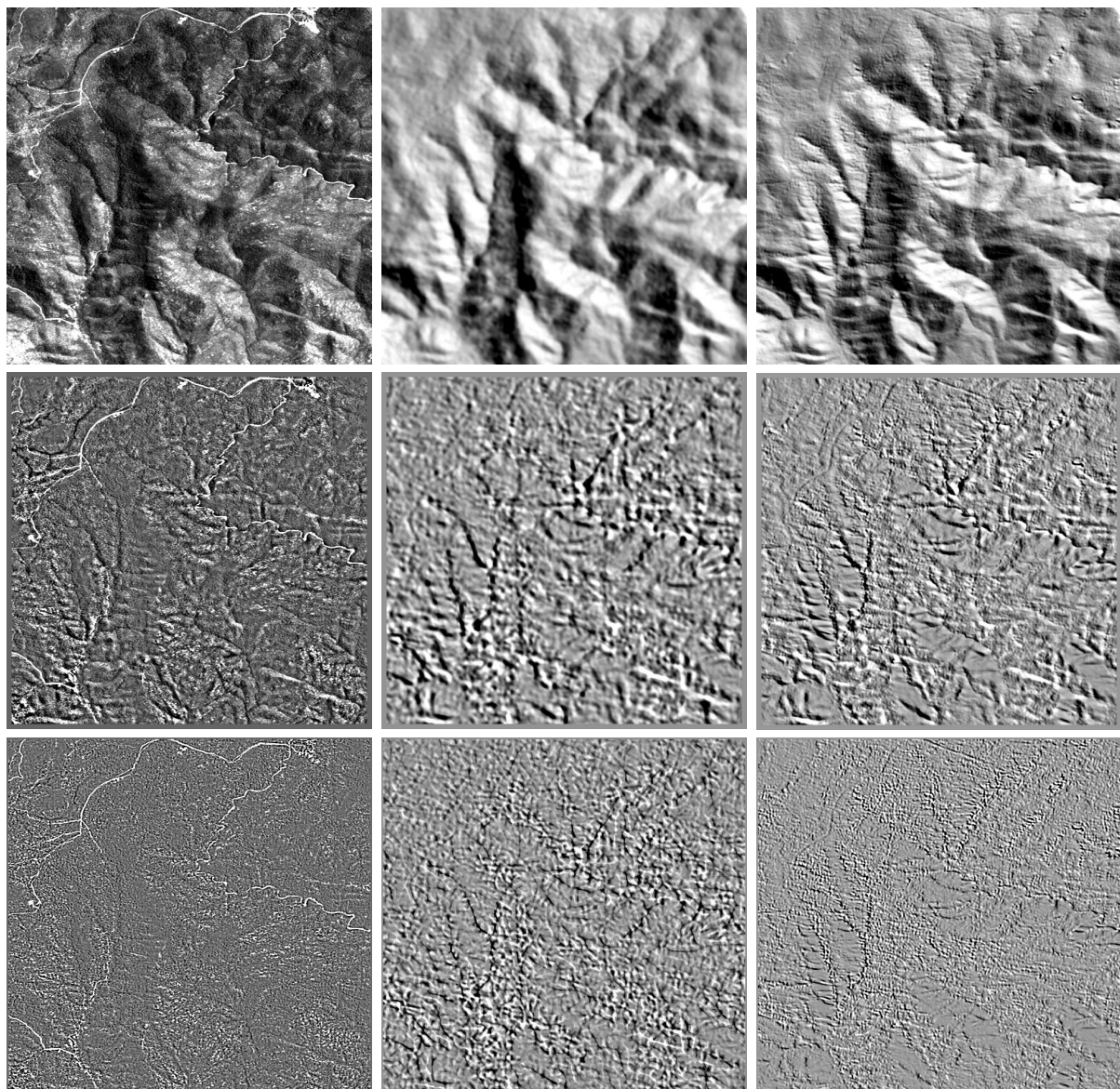


Figure 4.23 Landsat band 8 (left column), cosit from SRTM30 (middle column) and cosit from IDEM12 (right column) for unfiltered (top row), filtered with $kf = 19$ (middle row) and filtered with $kf = 11$ (bottom row)

These results suggest that neither Landsat panchromatic band nor the IDEM12 data at its finest resolution have information to the level suggested by their resolution and could perhaps be as well represented by (say) a 20m product. This is consistent with the visual analysis made before and needs some further research.

Overall, unlike the comparison between 90m SRTM and 30m SRTM, the two DEMs involved here are both useful to match Landsat data and be candidates for use in operational processing of Landsat data. Our analyses show that IDEM data have more spatial details than SRTM at the same resolution and correct many fine detail shadows missed by SRTM data. But making full use of this advantage also depends on the accuracy of operational geo-registration and other factors that are not specifically related to DEM quality.

5 Conclusions & Evaluation

We have found that if the most obvious noise issues can be addressed or avoided, then for the purposes of terrain correction of remote sensing data such as Landsat, results using IDEM data are generally consistent with those based on the currently used SRTM based data but can resolve Landsat shading effects at a finer scale than the SRTM data has been able to achieve. Therefore, provided the noise issues can be resolved, IDEM scale data could provide a basis for an operational product that can replace SRTM for terrain correction of data at Landsat resolution as well as finer scales (such as Landsat data at Panchromatic resolution). Note that similar effects in SRTM data were originally present but effectively removed making the possibility of improvement quite likely and the analysis reported here is not a judgement on IDEM terrain or roughness height data but only of the effectiveness of using the gradient field in the application described.

Both terrain illumination correction and filter bank analysis show that IDEM12 and IDEM30 in general deliver these better results when compared with SRTM30, with IDEM12 being the better of the two. The “better” in this case is based on the criterion that they resolve finer scales of detail in terrain shading in Landsat data than SRTM based DEM/DSMs. Previous work (Li et al., 2012, 2013) has shown that SRTM based data are not able to represent all of the terrain based variation found in Landsat data. However, the remaining noise issues in the IDEM data are likely to be the biggest limitation to its replacing SRTM based processing in operational use at this stage. An interesting result of significance to the current developments of next-generation 10-15m resolution DEM/DSM data is that using IDEM12 data aggregated to the resolution of the Landsat data is a better input to use than the IDEM30 resampled to match the Landsat resolution. But this method will only be available when higher quality IDEM12 or other similar scale DEM/DSM data are made operationally available in the future.

Whether IDEM12 data can consistently remove terrain shadow more efficiently than resampled SRTM data at a similar resolution to the panchromatic band would also need further investigation. The further investigation does not (however) just involve DEM analysis. Based on this study, it is questionable whether either Landsat panchromatic data or IDEM12 data at 12 m scale are truly at a scale expected of their nominal resolution. It is possible that they are both oversampled and the scale dependent signal versus noise properties of both IDEM12 data and Landsat Panchromatic data are yet to be fully established at this level. Such studies will need an area where well established base DEM data are available at a finer scale – such as may be available from Lidar and /or detailed ground survey.

Since the IDEM data provided for the study are an intermediate data product, spikes and noise, especially those associated with water covered areas, were still present in the data and they certainly need to be fixed before the data can be offered or used for operational purposes. SRTM data have clearly faced a similar problem and been fixed by methods that are not fully known to the authors of this study. For inland lakes, SRTM provides a flat surface at an elevation contour that seems reasonable for a lake or dam. We assume that by the time the WorldDEM™ is made available this issue will have been fixed and data will be available with similar worldwide coverage to SRTM. It is also possible that for some other gradient based products, such as streamlines and other hydrological information, further noise filtering may still be needed.

Acknowledgements

This report has been published with the permission of the CEO, Geoscience Australia. The authors wish to thank the German Aerospace Center (DLR, Project number: IDEM_OTHER0199) for providing the TanDEM-X IDEM data over Tasmania for this study and Drs Matt Garthwaite and Ken Lawrie of Geoscience Australia for reviewing this Record. The SRTM and Landsat datasets were provided by Geoscience Australia.

References

- Castleman, K. R. (1996). *Digital Image Processing*. Prentice-Hall signal processing series, Prentice-Hall, 667pp.
- Gallant, J. C., Dowling, T. I., Read, A.M., Wilson, N., Tickle, P., and Inskeep, C. 2011. 1 Second SRTM Derived Digital Elevation Models User Guide. Canberra: Geoscience Australia.
<http://www.ga.gov.au/topographic-mapping/digital-elevation-data.html>
- Horn, B.K.P. and Bachman, B.L. (1978). Using synthetic images to register real images with surface models. *Communications of the ACM*, 21, 914-924.
- Huber, M, Gruber, A., Wendleder, A., Wessel, B., Roth, A., and Schmitt, A., 2012. The TANDEM-X DEM: Production status and first validation results. *International Archives of the Photogrammetry, Remote Sensing and Spatial Information Sciences*, Volume XXXIX-B7, 2012 XXII ISPRS Congress, 25 August – 01 September 2012, Melbourne, Australia
- Iqbal, M. (1983). An introduction to solar radiation. Academic, New York, pp 390
- Kalnay, E., Kanamitsu, M., Kistler, R., Collins, W., Deaven, D., Gandin, L., Iredell, M., Saha, S., White, G., Woollen, J., Zhu, Y., Chelliah, M., Ebisuzaki, W., Higgins, W., Janowiak, J., Mo, K.C., Ropelewski, C., Wang, J., Leetmaa, A., Reynolds, R., Jenne, R. and Joseph, D.(1996). The NCEP/NCAR 40-Year Reanalysis Project. *Bulletin of the American Meteorological Society*, 77, 437-471
- Li, F., Jupp, D.L.B., Reddy, S., Lymburner, L., Mueller, N., Tan, P. and Islam, A. (2010). An evaluation of the use of atmospheric and BRDF correction to standardize Landsat data. *The IEEE Journal of Selected Topics in Applied Earth Observations and Remote Sensing*, 3, 257-270
- Li, F., Jupp, D.L.B., Thankappan, M., Lymburner, L., Mueller, N., Lewis, A. and Held, A. (2012). A physics-based atmospheric and BRDF correction for Landsat data over mountainous terrain. *Remote Sensing of Environment*, 124, 756-770
- Li, F., Jupp, DLB and Thankappan, M. 2013. Issues in the application of Digital Surface Model data to correct the terrain illumination effects in Landsat images, *International Journal of Digital Earth*, DOI: 10.1080/17538947.2013.866701
- Qin, Y. and Mitchell, R.M., 2012. Accurate aerosol remote sensing over bright land surfaces using AATSR, Proceeding of IGARSS 2012, Munich, 22-27 July, 2012
- Schaaf, C., Gao, F., Strahler, A.H., Lucht, W., Li, X., Tsang, T., Strugnell, N.C., Zhang, X., Jin, Y., Muller, J.-P., Lewis, P., Barnsley, M., Hobson, P., Disney, M., Roberts, G., Dunderdale, M., Doll, C., d'Entremont, R.P., Hu, B., Liang, S., Privette, J.L. and Roy, D. (2002). First operational BRDF, albedo and nadir reflectance products from MODIS. *Remote Sensing of Environment*, 83: 135-148.
- Shepherd, J.D. and Dymond, J.R. (2003). Correcting satellite imagery for the variance of reflectance and illumination with topography. *International Journal of Remote Sensing*, 24, 3503-314
- Wang, X. and Yin, Z. (1998). A comparison of drainage networks derived from digital elevation models at two scales. *Journal of Hydrology*, 210, 221-241.
- Wolock, D. M. and McCabe, G. J. (2000). Differences in topographic characteristics computed from 100- and 1000-m resolution digital elevation model data. *Hydrological processes*, 14, 987-1002.
- Yin, Z. and Wang, X. (1999). A cross-scale comparison of drainage basin characteristics derived from digital elevation models. *Earth surface processes and landforms*, 24, 557-5